Fermi National Accelerator Laboratory

FERMILAB-FN-627

Beam-beam Interaction Effects in the Fermilab Collider

Donna Marie Siergiej

B.S., Eisenhower College of the Rochester Institute of Technology, 1981
M.S., University of New Mexico, 1986

DISSERTATION

Submitted in Partial Fulfillment of the
Requirements for the Degree of

Doctor of Philosophy in Physics

The University of New Mexico
Albuquerque, New Mexico

March 1995

Operated by Universities Research Association Inc. under Contract No. DE-AC02-76CHO3000 with the United States Department of Energy

Disclaimer

BEAM-BEAM INTERACTION EFFECTS IN THE FERMILAB COLLIDER

BY

DONNA MARIE SIERGIEJ

B.S., Eisenhower College of the Rochester Institute of Technology, 1981

M.S., University of New Mexico, 1986

DISSERTATION

Submitted in Partial Fulfillment of the
Requirements for the Degree of

Doctor Of Philosophy in Physics

The University of New Mexico

Albuquerque, New Mexico

March 1995

*This work has been supported by Fermi National Accelerator Laboratory under the Joint University-Fermilab Doctoral Program in Accelerator Physics. Fermilab is operated by the Universities Research Association under contract with the United States Department of Energy.

For my parents,
Walter and Eileen Siergiej

ACKNOWLEDGEMENTS

I extend my gratitude to Robert Joshel, whose friendship and encouragement inspired me to complete this work.

I would like to thank the director of Fermi National Accelerator Laboratory, John Peoples, for giving me the opportunity to study beam-beam interaction effects in the Tevatron Collider. I also thank my academic advisor at the University of New Mexico, David Wolfe, for his guidance and support.

In the course of my graduate research program, I have had the fortune of working with three research advisors, each of whom contributed in part to my learning the tools of the trade. I thank Glenn Goderre, Rol Johnson and Edl Schamiloglu for the valuable time I spent working with them. I also thank Glenn Goderre for his comments and suggestions during the writing of this dissertation.

I am grateful to Leo Michelotti and Steve Peggs for helping me gain an understanding of the beam-beam interaction. I would also like to thank Werner Herr for his assistance in developing a beam-beam simulation of the Tevatron during my visit to CERN.

There are many people in the Accelerator Division at Fermilab whom have helped me in a steady manner. Most importantly, I wish to acknowledge the Operations Staff for their selfless help during my beam studies in the Tevatron. I was constantly impressed by their willingness and enthusiasm to work on any projects or problems which would arise. My discussions with Peter Bagley, Jerry Annala, Mike Martens and Norman Gelfand of the Tevatron group always proved helpful. Linda Spentzouris and Francois Ostiguy were both colleagues and friends during my stay at Fermilab, and I thank them for their valuable advice and assistance.

I would especially like to thank David Finley for his active interest in this work and for sharing his methods of scientific inquiry.

BEAM-BEAM INTERACTION EFFECTS IN THE FERMILAB COLLIDER

BY
DONNA MARIE SIERGIEJ

ABSTRACT OF DISSERTATION

Submitted in Partial Fulfillment of the
Requirements for the Degree of

Doctor Of Philosophy in Physics

The University of New Mexico
Albuquerque, New Mexico

March 1995

BEAM-BEAM INTERACTION EFFECTS IN THE FERMILAB COLLIDER

DONNA MARIE SIERGIEJ

Ph.D., Physics, University of New Mexico, 1995

Fermi National Accelerator Laboratory's Collider is the first collider to implement a helical orbit separation scheme for colliding protons and antiprotons. Six antiproton bunches collide head-on with six proton bunches at the two high energy physics detector locations in the ring. The orbits are separated in both the horizontal and vertical planes at all other collision points.

A study of the dependence of the beam-beam interaction on transverse beam separation is presented. Beam-beam experiments in the Collider determined that the beam-beam interaction is the predominant nonlinear force which drives seventh order resonances in the Collider. These odd-ordered resonances were observed to cause large particle losses in the presence of a transverse beam separation or crossing angle at an interaction point. This observation led to a method of "helical orbit tuning" using electrostatic separators and resulted in a 5% increase in the luminosity during Collider Run IA. Independant tuning of beam separation and crossing angle at head-on collision points now provides a luminosity enhancement in routine Collider operations.

Beam-beam experiments were compared with beam-beam simulations to produce an understanding of colliding beam behavior when two particle distributions collide with a transverse beam separation. An experimental measure of particle losses due to resonant excitation at different beam separations showed good agreement with beam-beam simulation results. This comparative agreement extends across a range of beam separations and particle tunes.

This investigation lays a foundation for using beam-beam simulations as a predictive tool for defining minimum beam separation criteria for stable Collider operation.

Contents

1 INTRODUCTION 1

2 PARTICLE MOTION IN AN ACCELERATOR 4

2.1 Relevant Accelerator Physics Parameters 4

2.2 Resonant Motion due to Magnetic Field Errors 18

2.3 The Tevatron as a Collider 21

2.4 Accelerator Parameters during Collider Runs IA and IB 23

3 THE BEAM-BEAM INTERACTION 28

3.1 The Beam-beam Force 28

3.2 A Hamiltonian Analysis 30

The Unperturbed Hamiltonian 32

The Resonant Hamiltonian 33

3.3 The Beam-beam Tune Shift 34

3.4 Amplitude of a Resonance 38

3.5 Beam-beam Simulations 42

4 EXPERIMENTAL METHODS OF MEASUREMENT 47

4.1 Measurement of the Tune 47

4.2 Background Losses 48

4.3 Luminosity 50

4.4 Bunch Intensities and Longitudinal Bunch Length 51

4.5 Transverse Beam Sigma and Beam Emittance 53

The Flying Wires 53
The SVX at CDF 55

5 BEAM-BEAM EXPERIMENTS IN THE TEVATRON 57
5.1 ORBIT CONTROL AT AN INTERACTION POINT 57
Four-Bumps using the Separators 58
Luminosity vs. Separation and Crossing Angle 60
5.2 IDENTIFYING BEAM-BEAM DRIVEN RESONANCES 69
Proton Losses during Tune Scans 71
5.3 INVESTIGATING BEAM-BEAM DRIVEN RESONANCES AS A FUNCTION OF BEAM SEPARATION 74
Collider Run IA - A Beam-beam Experiment and Problems with the Measurement 76
Collider Run IB - Measurement of Particle Losses as a Function of Transverse Beam Separation 78
5.4 COMPARISON WITH A BEAM-BEAM MODEL 85
Definition of a Lost Particle 88
Definition of Maximum % Smear 90
Simulations of a 1x1 Store in the Tevatron 92

6 CONCLUSIONS 109

7 APPENDICES 111

A ORBIT CONTROL OF BEAM SEPARATION AND CROSSING ANGLE AT AN INTERACTION POINT 112

B LUMINOSITY AS A FUNCTION OF SEPARATION AND CROSSING ANGLE 117

C A HISTORICAL REVIEW OF THE USE OF ELECTROSTATIC SEPARATORS IN COLLIDERS 121

BIBLIOGRAPHY 124

List of Tables

2.1 Tevatron Accelerator Parameters in Collider Run IA and IB 24
2.2 Tevatron Lattice Parameters in Collider Run IA and IB 25

5.1 Normalized emittance and longitudinal bunch length used in a calculation of transverse overlap 65
5.2 Comparison of transverse overlap measurements 66
5.3 Measured proton tune in Collider Run IB beam-beam experiment 79
5.4 Bunch intensities in Collider Run IB beam-beam experiment 83
5.5 Resonant tunes in a vertical tune scan simulation 98

A.1 Separator lattice parameters in Collider Run IA 116

List of Figures

2.1 Layout of Fermilab's accelerators 5
2.2 Coordinate system to define a particle's closed orbit. 6
2.3 Phase space transformation of a linear one-dimensional turn-by-turn map 11
2.4 Phase plot of a linear one-dimensional turn-by-turn map with a constant gradient error 14
2.5 Resonance lines in tune space 15
2.6 Horizontal and vertical beta function at the CDF interaction region 22
2.7 Beta wave in a section of the Tevatron in Collider Run IA 26

3.1 Angular deflection due the beam-beam interaction 30
3.2 Horizontal and vertical tune shift due to beam-beam detuning 36
3.3 Beam-beam tune footprint for one head-on collision in the Tevatron Collider 38
3.4 Absolute value of the amplitude of a beam-beam driven resonance for head-on collisions 40
3.5 Amplitude of a beam-beam driven resonance for head-on collisions 40
3.6 Absolute value of the amplitude of a beam-beam driven resonance for a beam separation of 2σ. 41
3.7 Amplitude of a beam-beam driven resonance for a beam separation of 2σ . 41
3.8 Amplitude of a beam-beam driven resonance of $7th$ order for different horizontal separations 42
3.9 Beam-beam simulation calculation of tune shift in the presence of a non-zero horizontal separation 46

4.1 Tune spectrum measured from horizontal Schottky plates in the Tevatron . 47
4.2 A sketch of one half of the CDF detector 49
4.3 Transverse view of a Bunched Beam Counter at CDF. 50

4.4 The Resistive Wall Monitor in the Tevatron. 51
4.5 The Sampled Bunch Display 52
4.6 Sketch of a flying wire assembly. 53
4.7 Flying Wire transverse profiles of a proton and antiproton bunch as measured by the flying wires 54
4.8 The SVX detector at CDF. 56

5.1 Sketch of the location of the separators in the Tevatron 58
5.2 A model's prediction of beam positions in the Tevatron due to a crossing angle bump at B0. 59
5.3 An orbit difference between two measured orbits in the Tevatron: a "four-bump on" minus a "four-bump off" orbit. 59
5.4 A model's prediction of orbit displacements at the BPMs in the Tevatron due to a separation bump at B0 61
5.5 Sketch of the variation of transverse sigma of two colliding bunches in longitudinal space 62
5.6 A MINUIT fit of measured luminosity vs. vertical beam separation at B0 . 63
5.7 A MINUIT fit of measured luminosity vs. horizontal beam separation at B0 64
5.8 Primary vertex data as measured by the SVX at the B0 interaction point . 67
5.9 Three dimensional view of SVX primary vertex data 67
5.10 A MINUIT fit of measured luminosity vs. horizontal crossing angle at B0 68
5.11 Map of experimental tune scans in tune space 70
5.12 Comparison of measured background losses at the B0 and D0 interaction regions during a tune scan 71
5.13 Proton losses measured at B0 while crossing the 5th and 8th order resonances 72
5.14 Proton losses measured at B0 while crossing the 7th order resonance . . . 73
5.15 Background Losses as a function of vertical proton tune for three tune scans during Collider Run IA 75
5.16 Particle losses during a change of tune 77
5.17 Proton tune settings where particle losses were measured during the beam-beam experiment of Collider Run IB 78
5.18 A close-up of Figure 5.17 79

5.19 Antiproton background losses at B0 when the proton tune is near the 7th, 9th and 11th order resonances of Figure 5.18 81
5.20 Proton background losses at B0 when the proton tune is near the 7th, 9th and 11th order resonances of Figure 5.18 82
5.21 Tune diagram marking the measured proton tune settings of the beam-beam experiment and the base tune of particles which are unperturbed by the beam-beam interaction. 83
5.22 Antiproton losses and lifetimes at different beam separations 86
5.23 Proton losses and lifetimes at different beam separations 87
5.24 Effect of different amplitude limits on simulated particle losses in a vertical tune scan 89
5.25 Observed resonances in a simulated vertical tune scan 91
5.26 Effect of the beam-beam interaction on one-dimensional motion in phase space 92
5.27 Maximum horizontal and vertical % smear in a simulated vertical tune scan 93
5.28 Antiproton beam-beam tune footprints of Measurement 1 96
5.29 Antiproton beam-beam tune footprints of Measurement 2 97
5.30 Simulated particle losses for Measurement 1 and Measurement 2 99
5.31 Simulated maximum % smear for Measurement 1 and Measurement 2 . . 100
5.32 Comparison of measured particle losses to simulated particle losses for Measurement 2 101
5.33 Antiproton beam-beam tune footprints of Measurement 3 103
5.34 Simulated particle losses for Measurement 3 104
5.35 Comparison of measured particle losses to simulated particle losses for Measurement 3 105
5.36 Simulated maximum % smear for Measurement 3 107
5.37 Antiproton beam-beam tune footprints of Measurement 4 108

A.1 Schematic of a four-bump 113

B.1 Schematic of two bunches colliding with a crossing angle 120

Chapter 1

INTRODUCTION

The goal of accelerator physics in hadron colliders is to provide a large number of interactions of colliding particles at a large center of mass energy (TeV range). Collisions of particles at such high energies allow high energy physicists to look for interactions which will further their understanding of the strong force and the elementary particles subjected to this force.

The number of interactions per second of two colliding distributions of particles is defined as

$$R = \mathcal{L}\,\sigma_{\text{tot}} \tag{1.1}$$

where $\mathcal{L}$ is the luminosity and σ_{tot} is the total nuclear cross section. The total nuclear cross section is the cross sectional area of collisions, given in units of square cm. Luminosity is the number of interactions per square cm per second.

In order to provide a large number of interactions, an accelerator physicist works at optimizing the luminosity. It will be shown in this work that the luminosity of two colliding particle distributions of equal transverse size is

$$\mathcal{L} = \frac{N_1 N_2 f_{rev}}{4\pi\sigma^2} F(z). \tag{1.2}$$

The particle distributions are assumed to be Gaussian distributions with a standard deviation given by σ. The revolution frequency is f_{rev} and $F(z)$ is a factor taking into account the longitudinal distribution of the bunches. The number of particles in the two colliding distributions are given by N_1 and N_2, respectively.

A particle distribution is confined and accelerated in a synchrotron with an externally

applied RF field, which bunches particles into discrete time-dependent distributions. If there are multiple bunches colliding in an accelerator, the total luminosity is

$$\mathcal{L}_{total} = \mathcal{L}B \tag{1.3}$$

where B denotes the number of bunches.

The beam-beam interaction is the electromagnetic interaction a particle experiences as it travels past an opposing particle distribution. Two colliding bunches in a synchrotron will experience a beam-beam interaction at two points in the ring. Multiple bunches in a synchrotron will increase the number of beam-beam interaction points.

The beam-beam interaction between colliding particles has been a dominant factor in limiting the integrated luminosity in a colliding beam storage ring. Efforts to curb measureable luminosity limitations due to the beam-beam interaction seem to have led quite naturally to an implementation of beam separation schemes in storage rings. Particles of opposite charge were separated in the VEPP-2 electron-positron storage ring at Novosibirsk as early as 1967.[1]

In the first Collider Run (1988-1989) of Fermilab's hadron collider known as the Tevatron, the principle limitation on the luminosity was due to the beam-beam interaction. The Collider had reached its "beam-beam limit"; that is, one could not increase the luminosity by decreasing the beam size or by increasing the number of protons per bunch.[2] In fact, it was necessary to dilute the phase space density of the protons in order to maintain antiproton stability. In order to decrease beam-beam effects at unwanted collision points, a method of separating colliding bunches at certain locations in the ring was developed. This became necessary in order to progress to a higher luminosity.

A helical orbit separation scheme was first implemented in the Collider in Collider Run IA (1992-1993). Six antiproton bunches and six proton bunches were separated at every beam-beam collision point except for the two crossing points at the high energy physics detector locations. Colliding beams moved in helical orbits with beam separation present in both the horizontal and vertical planes. The achievable luminosity of $1.6 \times 10^{30}\text{cm}^{-2}$ sec^{-1} without beam separation increased to luminosities of $5.4 \times 10^{30}\text{cm}^{-2}$ sec^{-1} in routine operations during Collider Run IA.[3]

This dissertation presents a study of the dependence of the beam-beam interaction on transverse beam separation. A method of tuning the helical orbit in order to optimize the luminosity is discussed. Experiments performed in the Tevatron Collider measured particle losses as a function of beam separation. A comparison is made between experimentally

measured losses and the dynamics of a particle's motion in a simulation code which models the beam-beam interaction. Particle losses in a real accelerator are related to losses as defined in the model. The similarities along with the discrepancies between the measurements and the beam-beam simulation are discussed. Observations are made concerning the predictive power of a beam-beam model.

Chapter 2 contains a brief description of relevant accelerator physics parameters used throughout this work. A Hamiltonian analysis of the beam-beam interaction is discussed in Chapter 3, along with an introduction of the beam-beam simulaton code. Chapter 4 describes various devices in the Tevatron which were used as measuring tools in beam-beam experiments. Chapter 5 presents the results of beam-beam experiments in the Tevatron and compares the experimental results to beam-beam simulations. Chapter 6 concludes the beam-beam study with a summary of the results.

Chapter 2

PARTICLE MOTION IN AN ACCELERATOR

A particle accelerator uses combinations of focusing and defocusing magnetic elements to define a stable orbit for accelerating particles. This system of strong focusing is known as an alternating gradient system.[4] Particle motion under the influence of an alternating gradient system in the Tevatron Collider is the subject of this chapter.

A reader's knowledge of accelerator physics terminology is not assumed, so accelerator physics concepts relevant to this work are defined. Section 2.1 provides a brief description of the dynamics of a single particle's motion. The fundamentals of particle motion in the presence of magnetic field errors is discussed in Section 2.2.

This dissertation presents beam-beam experiments performed in Fermilab's Tevatron during a Collider Run (Collider Run IA and Collider Run IB). Section 2.3 is intended to introduce the reader to the Tevatron as it is used during a Collider Run. Section 2.4 lists the operational accelerator physics parameters relevant to the beam-beam experiments.

2.1 RELEVANT ACCELERATOR PHYSICS PARAMETERS

The Fermilab Tevatron has the distinction of being the highest energy collider in existence, currently colliding proton and antiprotons at a center of mass energy of 1800 GeV. The ability to constrain such high energy particles in a 1 km radius ring is due to the bending and focusing capabilities of the superconducting magnets.[5] The Tevatron was the first accelerator to make use of superconducting magnets.[6] All of the dipole, quadrupole and correction magnets are cooled to 4.6 degrees Kelvin, enabling maximum electric current to flow through coils with minimal resistance.

An overview of the Fermilab accelerator complex is shown in Figure 2.1.[7] The Tevatron is divided into six sectors called arcs which are connected by six long straight sections.

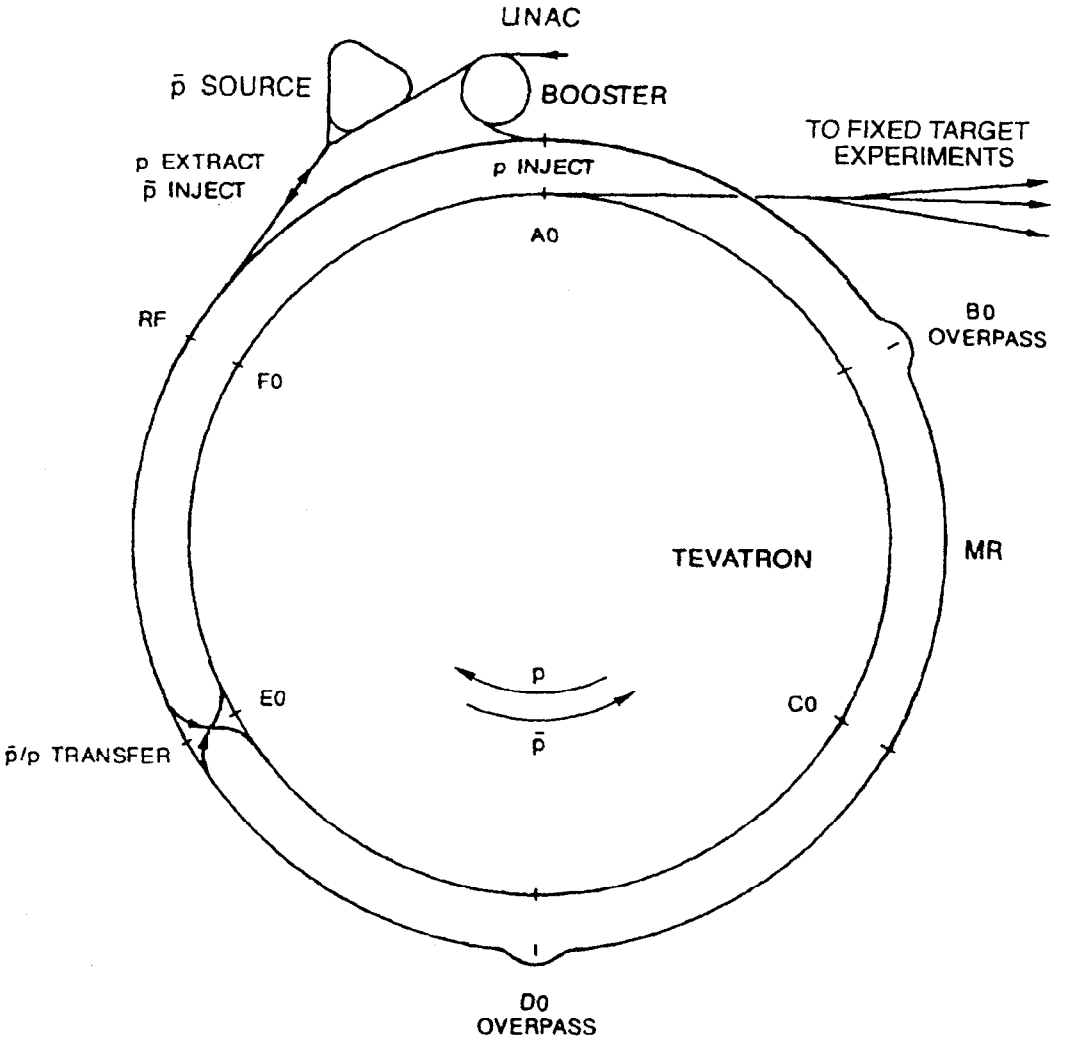

Figure 2.1: Layout of Fermilab's accelerators. The relative size of the accelerators is approximately to scale except that the Tevatron is actually built below the Main Ring. The radius of the Main Ring and Tevatron is 1 km. High energy physics detectors are located at the B0 and D0 straight sections.

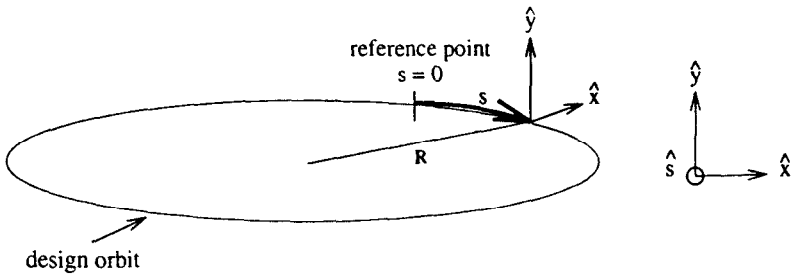

Figure 2.2: Coordinate system to define a particle's closed orbit.

The arcs are composed of a repeating sequence of "cells". The configuration of magnets in a cell is determined by the principles of an alternate-gradient focusing scheme. A typical half-cell in the Tevatron consists of four dipole magnets, a quadrupole and magnetic correction elements. The detailed description of the way in which dipoles, quadrupoles, drift sections and all of the correction elements are placed in the ring is called the accelerator "lattice".

The constant magnetic field of the dipole magnets in the arcs of the Tevatron guides a charged particle along an approximately circular orbit. If the particle travels through the center of the quadrupoles and correction elements, consequently being guided only by the dipole field, the particle's trajectory is said to follow the design orbit of the accelerator. Any particle whose path deviates slightly from the design orbit is focused onto a closed orbit by quadrupole magnets.

It is convenient to define a reference frame to describe a particle's closed orbit as shown in Figure 2.2. The $\hat{x}$ and $\hat{y}$ directions describe the horizontal and vertical deviations of the particle's motion from the design orbit. The $\hat{s}$ direction is the curvilinear coordinate indicating the direction tangential to the particle's forward motion. At high energies, the azimuthal location s is represented in the time domain as $s = ct$, c being the speed of light. The coordinate system is a right-handed coordinate system, so the positive sense of $\hat{x}$ points in the radially outward direction and $\hat{y}$ points in the vertically upward direction.

A quadrupole magnet produces a magnetic field which changes linearly in both transverse dimensions; $B_x = \frac{\partial B_x}{\partial y}\, y$ and $B_y = \frac{\partial B_y}{\partial x}\, x$. An approximation which is made in a high energy accelerator is a thin lens approximation: a particle travelling through a quadrupole will experience a negligible change in its position and experience only a small change in the transverse components of its momentum. In this approximation, a particle travelling through a short quadrupole of length L receives a small-amplitude kick which is given by

$$\Delta x' = -\frac{L}{|B\rho|} B_x \qquad \Delta y' = \frac{L}{|B\rho|} B_y. \tag{2.1}$$

The prime denotes a differentiation with respect to the longitudinal coordinate s; $x' \equiv dx/ds$. The constant dipole field guiding the particle in a circular orbit is given by B and the dipole bend radius is ρ. The quantity $|B\rho|$ is the momentum per unit charge of a particle ($|B\rho| = p/e$) and is called the magnetic rigidity. The quadrupole kick is focusing in the horizontal plane and it is defocusing in the vertical plane. It is possible to produce a net focusing system using a sequence of quadrupoles in which a quadrupole which is defocusing in a given plane is followed by a quadrupole which focuses in that plane. Such a system of alternating focusing and defocusing quadrupoles, along with the drift spaces in between the quadrupoles, form the basic elements of an alternating gradient system.[4]

The Lorentz force, $e\vec{v} \times \vec{B}$, describes the motion of a particle in the presence of the dipole magnets, quadrupole magnets and drift sections of a synchrotron. The equation of motion derived from this force is known as Hill's equation. In one dimension, Hill's equation is[4]

$$\frac{\partial^2 x}{\partial s^2} + K(s)x = 0. \tag{2.2}$$

The deviation of a particle's motion from its closed orbit is given by $x(s)$. The quadrupole strength is $K(s)$, where

$$K(s) = \pm \frac{1}{B\rho} B'(s). \tag{2.3}$$

The magnetic field at the azimuthal point s is $B(s)$. The gradient of the quadrupole field, $B' = \partial B_y/\partial x = \partial B_x/\partial y$, is equal in both transverse planes as described by Maxwell's expression for the curl of B in free space, $\nabla \times \vec{B} = 0$. Note that $K(s)$ is zero in a drift section and is also zero in a dipole if one neglects magnetic field errors. In a circular accelerator, the quadrupole strength is periodic with the circumference of the accelerator. It also alternates in sign depending upon whether the quadrupole is focusing or defocusing in a given plane.

In general, K(s) may be taken as a constant for each magnetic element in the ring. At 1 TeV, a standard focusing quadrupole in the Tevatron operates with a magnetic field gradient of 76 T/m, yielding a quadrupole strength of 0.02277 m^{-2}. The linear motion of a particle through each element in the ring can be solved for analytically in Hill's equation if the initial position and angle of the particle are known. Let the initial position and angle of a particle be x_1 and x_1' and its final position and angle after traversing a magnetic element of length L

be x_2 and $x_2^{'}$. The motion of the particle through the magnetic element is described by

$$\begin{pmatrix} x_2 \\ x_2^{'} \end{pmatrix} = M_{12} \begin{pmatrix} x_1 \\ x_1^{'} \end{pmatrix} \tag{2.4}$$

where M_{12} is a linear transfer matrix. The linear transfer matrices for quadrupoles ($K \neq 0$), drift sections ($K = 0$) and dipoles ($K = 0$) of length L are listed here.

$$K = 0: \quad M_{12} = \begin{pmatrix} 1 & L \\ 0 & 1 \end{pmatrix} \tag{2.5}$$

$$K \neq 0: \quad M_{12} = \begin{pmatrix} \cos(L\sqrt{K}) & \frac{1}{\sqrt{K}} \sin(L\sqrt{K}) \\ -\sqrt{K} \sin(L\sqrt{K}) & \cos(L\sqrt{K}) \end{pmatrix} \tag{2.6}$$

The focusing scheme used in accelerators is comparable to a combination of thin lenses in an optical system. In other words, the length of a quadrupole is much smaller than its focal length. Using the thin lens approximation, the length of the quadrupole in the linear transfer matrix of Equation 2.6 is assumed to go to zero as the quantity $\sqrt{K}\ L$ remains finite. The transfer matrix of a focusing quadrupole under the thin lens approximation is

$$M_{12} = \begin{pmatrix} 1 & 0 \\ -\frac{1}{f} & 1 \end{pmatrix}, \tag{2.7}$$

where $f = (KL)^{-1}$. The transfer matrix of a focusing quadrupole is none other than that of a thin optical focusing lens with focal length f. As shown previously, the same quadrupole will be defocusing in the other transverse plane of motion. A defocusing transfer matrix is equivalent to the focusing transfer matrix described above with the sign of f reversed, corresponding to a thin defocusing lens in an optical system. A standard quadrupole of length 1.678 meters in the Tevatron has a focal length of 26.1 meters. Thus the longitudinal distance between focusing and defocusing quadrupoles in the Tevatron is approximately 26 meters to provide net focusing in both transverse planes of motion.

ACCELERATOR LATTICE PARAMETERS

If a particle traverses a series of n elements having transfer matrices M_1,M_2,M_3 up to M_n, the motion through the elements is described by a single linear transfer matrix:

$$M_{12} = M_1 M_2 M_3 .... M_n. \tag{2.8}$$

This method of solution is useful in the design of a ring, but it is cumbersome to use in describing the general nature of particle trajectories. A much more convenient solution of Hill's equation is given by the general solution for x(s):

$$x(s) = A\sqrt{\beta(s)}\cos(\psi(s) + \delta). \tag{2.9}$$

The functions $\beta(s)$ and $\psi(s)$ are predetermined functions of s while A and δ are constants which determine a particular particle trajectory. Note that Hill's equation is the equation of motion of a harmonic oscillator with a periodic spring constant which depends upon distance. As would be expected, its solution resembles that of a harmonic oscillator except that the amplitude of oscillation is no longer constant but varies with distance.

A better understanding of the beta function, $\beta(s)$, and the phase advance of a particle, $\psi(s)$, is obtained by substituting x(s) into Hill's equation. Two differential equations become apparent,

$$\frac{\partial}{\partial s}(\beta\psi') = 0, \tag{2.10}$$

and

$$2\beta''\beta - (\beta')^2 - 4\beta^2(\psi')^2 + 4\beta^2K(s) = 0. \tag{2.11}$$

As Equation 2.11 indicates, if the focusing strength $K(s)$ is known, a solution for the beta function, $\beta(s)$, is found numerically. The beta function thus represents an alternative description of the magnetic focusing structure of the accelerator. It is a powerful representation in that it bypasses the necessity to always map a particle through all of the individual magnetic elements in the ring. The focusing properties of the entire ring are represented by the beta function in each transverse plane.

Equation 2.10 gives the phase advance of a particle's motion. A particle's phase advance from a location s_1 in the ring to a location s_2 is

$$\Delta\psi = \int_{s_1}^{s_2} \frac{ds}{\beta(s)}. \tag{2.12}$$

The phase advance of a particle does not change with a constant frequency like that of a harmonic oscillator. It increases as a function of the beta function or, equivalently, as a function of quadrupole strengths. The phase advance of a particle is defined in both the horizontal and vertical planes. In a given transverse plane, the beta function in the arcs of the Tevatron is approximately 100 meters at the location of a focusing quadrupole and is approximately

30 meters at the location of a defocusing quadrupole. A particle's horizontal phase advances more rapidly at the location of a defocusing quadrupole.

The parameters $\beta(s)$ and $\psi(s)$ are conventionally called accelerator lattice parameters or Twiss parameters. Twiss parameters were used by Courant and Snyder to define a linear transfer matrix which mapped a particle's motion through any number of magnetic elements in an accelerator.[4] This linear transfer matrix represents a particle's complete traversal in one plane from a location s_1 to a location s_2. As in Equation 2.8, the transfer matrix is given by

$$M_{12} = \begin{pmatrix} \sqrt{\frac{\beta_2}{\beta_1}}(\cos\Delta\psi + \alpha_1 \sin\Delta\psi) & \sqrt{\beta_2\beta_1}\sin\Delta\psi \\ -\frac{1+\alpha_1\alpha_2}{\sqrt{\beta_1\beta_2}}\sin\Delta\psi + \frac{\alpha_1-\alpha_2}{\sqrt{\beta_1\beta_2}}\cos\Delta\psi & \sqrt{\frac{\beta_1}{\beta_2}}(\cos\Delta\psi - \alpha_2\sin\Delta\psi) \end{pmatrix}. \quad (2.13)$$

The parameter $\alpha(s) = -\frac{1}{2}(\partial\beta/\partial s)$ is an accelerator lattice parameter which describes the slope of the beta function.

The Tune of a Particle

The periodicity of the beta function with the circumference of the ring dictates that a particle will advance in phase by the same amount upon each revolution of the ring. This quantity is written as $2\pi Q$, where

$$Q = \frac{1}{2\pi}\oint \frac{1}{\beta(s)} ds. \quad (2.14)$$

The parameter Q is known as a particle's tune. The complete integral signifies that the integration is over one complete revolution of the ring. Inasmuch as the beta function is defined in two transverse planes, the tune of a particle is defined in two transverse planes. A particle's tune is an important quantity in accelerator physics and particularly in this work, so it will be discussed in some detail in this chapter and in later chapters.

Consider observing a particle's motion at only one azimuthal location in the ring. A particle's position and phase at one observation point can be mapped in terms of an integer turn number by equating the turn number t with the azimuthal coordinate s as $t \equiv s/2\pi R$. A particle's trajectory from turn $t-1$ to turn t is described by

$$\begin{pmatrix} x_2 \\ x_2' \end{pmatrix}_t = M \begin{pmatrix} x_1 \\ x_1' \end{pmatrix}_{t-1}. \quad (2.15)$$

The phase advance of a particle from turn $t-1$ to turn t is $\Delta\psi = 2\pi Q$. Referring to Equation 2.13, the one-turn transfer matrix M is constructed;

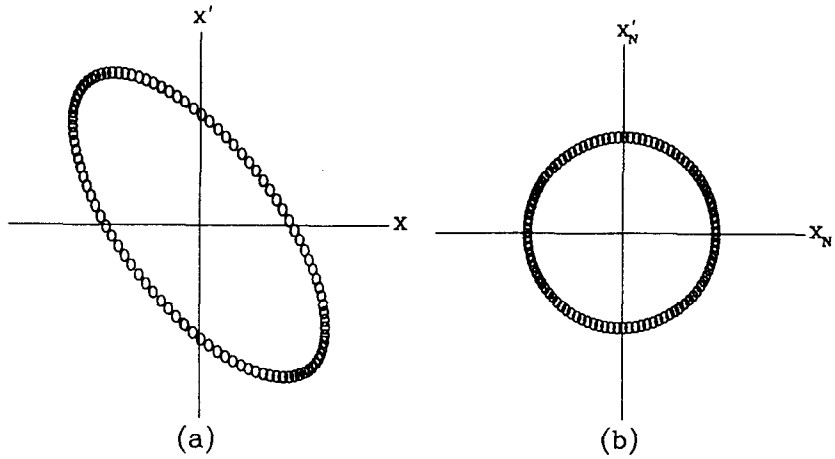

Figure 2.3: The phase space transformation of 100 turns of a linear one-dimensional turn-by-turn map from (x, x') coordinates to normalized (x_N, x'_N) coordinates.

$$M = \begin{pmatrix} \cos 2\pi Q + \alpha \sin 2\pi Q & \beta \sin 2\pi Q \\ -\frac{1+\alpha^2}{\beta} \sin 2\pi Q & \cos 2\pi Q - \alpha \sin 2\pi Q \end{pmatrix}. \tag{2.16}$$

The lattice parameters α and β are calculated using knowledge of the one-turn map, M.

Transverse Beam Emittance

A plot of a particle's position and phase at one location in the ring over the course of many turns is shown in Figure 2.3a. The particle's trajectory maps out an ellipse in the phase space coordinates (x, x'). The area of the ellipse is equal to πA^2, where A is a constant. This area is a constant of the motion, similar to the total energy of a harmonic oscillator. After calculating the derivative of x(s) with respect to s using Equation 2.9, the constant of the motion is found to satisfy

$$\frac{x^2 + (\beta x' + \alpha x)^2}{\beta} = A^2. \tag{2.17}$$

This equation points to a useful transformation from the (x, x') coordinate system to a normalized coordinate system (x_N, x'_N), where

$$\begin{aligned} x_N &= \frac{1}{\sqrt{\beta}} x \\ x'_N &= \frac{\alpha}{\sqrt{\beta}} x + \sqrt{\beta} x'. \end{aligned} \tag{2.18}$$

Since β and x are in units of meters, the normalized coordinates are in units of square root of a meter. This transformation is referred to as a Courant-Snyder transformation.[4] It is

based on the Floquet theory which ensures the existence of a periodic coordinate system which removes time dependence from the linear system.[8] By making this transformation, M now becomes a simple rotation matrix. As shown in Figure 2.3b, the motion of a particle over many turns traces out a circle in normalized phase space coordinates. Just as in the elliptical mapping, the area of the circle in phase space remains constant and equal to πA^2. In accelerator physics, this constant of the motion is known as the transverse emittance of a single particle.

Formally, transverse beam emittance is defined in terms of a distribution of particles. Transverse beam emittance is defined as the area of phase space in which a prescribed fraction of particles reside. With a measurement of the beam distribution in physical space at one location in the ring, the emittance enables calculation of the beam size at other azimuthal locations.

In the Tevatron, a valid approximation is to assume that a particle distribution in both the transverse and longitudinal dimensions is a Gaussian distribution, that is,

$$N(x) = \frac{N_0}{\sqrt{2\pi}\sigma} e^{-\frac{x^2}{2\sigma^2}} \tag{2.19}$$

in one dimension. The parameter $N(x)$ denotes the number of particles at a transverse position x. The total number of particles in the distribution is N_0. The rms beam size in physical space is given by σ. The beam emittance, ϵ, for a Gaussian distribution is

$$\epsilon = -\frac{2\pi\sigma^2}{\beta} \ln(1-f), \tag{2.20}$$

where the beta function and σ are defined at the same azimuthal location.[16] The units of emittance are *mm-mrad*. The fraction of particles contained within a given beam emittance is f. Determination of the fraction of particles to include in a definition of a beam size is somewhat arbitrary, hence different accelerator organizations choose different values of f. Fermilab chooses to include 95% of the particle distribution in phase space, yielding a beam emittance of

$$\epsilon = \frac{6\pi\sigma^2}{\beta}. \tag{2.21}$$

Since beam emittance is a constant of the motion, the value of σ^2/β remains constant in each transverse plane of motion around the entire ring. Thus, as Equation 2.9 indicates, an appropriately scaled beta function represents an envelope of the physical boundary that a beam distribution may encompass as it traverses the ring.

Beam emittance as defined above may not remain constant as the energy of the beam changes though. Liouville's theorem defines the phase space area which remains invariant over all particle energies.[11] In order to define this invariant, a transformation from (x, x') coordinates to the conjugate variables (x, p_x) is required. The variable p_x is the transverse component of the particle's momentum defined in one degree of freedom. The phase space area in terms of (x, p_x) coordinates is

$$\oint dp_x dx = mc\,(\gamma\beta)_{rel} \oint dx' dx = mc\,(\gamma\beta)_{rel}\,\epsilon. \tag{2.22}$$

Normalized emittance is given by

$$\epsilon_N = \frac{1}{mc} \oint dp_x dx = (\beta\gamma)_{rel}\,\epsilon. \tag{2.23}$$

Note that the subscript notation on the parameters β and γ indicate that these quantities are not accelerator lattice parameters. They are the familiar relativistic parameters; $\beta = v/c$ and $\gamma = 1/(1-\beta^2)$. The particle's rest mass is denoted by m. As defined above, normalized emittance is invariant over all particle energies. It is a measuring tool which is used very often to determine if the accelerator is running properly over its entire energy range.

Constraints on a Particle's Tune

The magnetic field in a magnetic element can be expressed as a series of multipole terms: the coefficient of the second order term ($n = 2$) represents the quadrupole field component, the coefficient of the third order term ($n = 3$) represents the sextupole field component of the magnetic field, and so forth (see Section 2.2). Upon passing through a magnetic element, a particle will experience a kick every revolution of the ring due to the sum of all field components in the magnetic element.

Consider the motion of a particle in one dimension with a tune satisfying the relation $nQ = p$, where n and p are integers. If $n = 2$ and the particle's tune is a half-integer value, the kick will add in phase and the particle's tune is on resonance. Similarly, if $n = 3$ and the particle's tune is a third integer value, a resonant condition exists. This argument extends to higher order magnetic field components as well. A resonant condition is equivalent to adding constant vectors parallel to the x'_N axis of phase space as shown in Figure 2.4. A particle's phase space history in the presence of a constant kick at a single location is mapped for a tune which is an odd multiple of one-half. The kick in x' in Figure 2.4a translates into a growth in x at a downstream location as seen in Figure 2.4b.

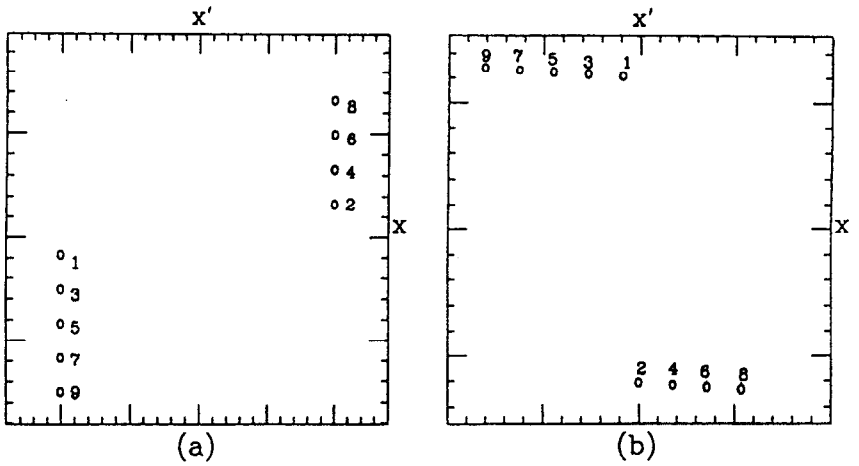

Figure 2.4: Phase plot of a linear one-dimensional turn-by-turn map of 9 turns with a constant kick in x' at one location. The particle's tune is near the half-integer. Figure a is the phase plot at the location of the kick. Figure b is the phase plot at a location $\pi/2$ downstream of the kick location. The turn number is labelled at each point in phase space.

After many turns, even a small kick in x' will cause growth in a particle's amplitude at a downstream location and will eventually lead to the loss of the particle. This resonance condition is defined in two transverse dimensions as

$$n_x Q_x \pm n_y Q_y = p. \tag{2.24}$$

The order of the resonance is given by summing the constants $|n_x| + |n_y|$. The integer p is the azimuthal frequency which drives the resonance.[12]

A plot of resonance lines satisfying Equation 2.24 is shown in Figure 2.5. The solid lines represent sum resonances and satisfy Equation 2.24 when both n_x and n_y are positive. The dashed lines represent difference resonances and satisfy Equation 2.24 when either n_x or n_y are negative.

If all resonance lines which satisfied Equation 2.24 were drawn in tune space, a countably infinite number of lines would fill the plot. It will be demonstrated in this work that only lower order resonance effects in the Tevatron are important to avoid. Consequently, only resonance lines up to twelfth order are drawn. The fractional tune used as a nominal operating point in the Tevatron Collider is marked in the tune plot. The horizontal and vertical operating tunes are amidst the region of 12th order resonances and are bordered by 5th and 7th order resonances.

The expression relating a magnetic field gradient error in an accelerator to the shift in

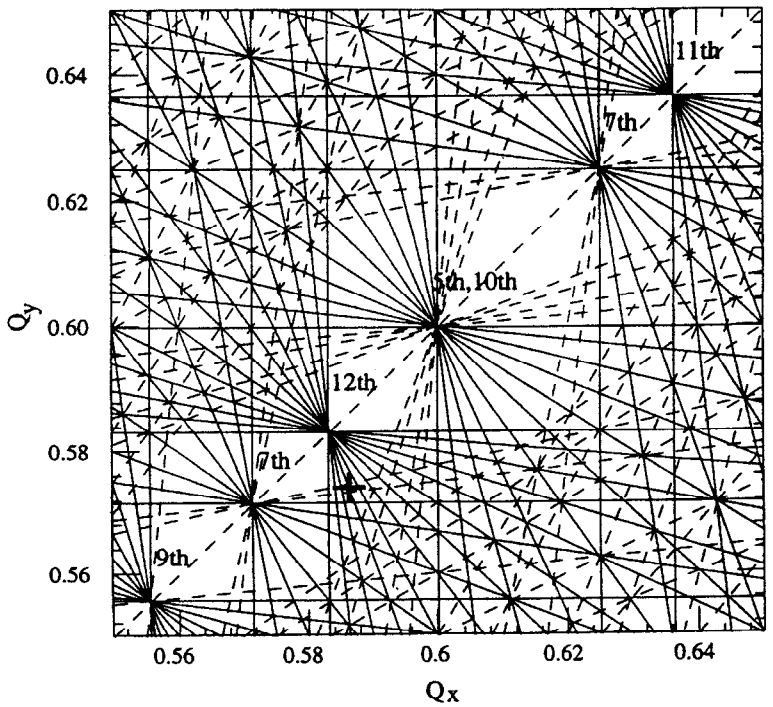

Figure 2.5: Resonance lines in tune space. Solid and dashed lines denote sum and difference resonances, respectively. Regions are labelled by the order of the sum resonances. The operating point of the Tevatron is indicated by the cross mark.

a particle's tune is found by comparing the one turn transfer matrix which includes a small gradient error to the transfer matrix of equation 2.16. The gradient error is expressed as the inverse focal length of a thin quadrupole; $q = \frac{1}{f} = KL$. The shift in a particle's tune due to a magnetic field gradient error q is

$$\Delta Q = \frac{1}{4\pi}\beta q, \tag{2.25}$$

where β is the beta function at the location of the gradient error.

In order to control the tune shift of particles due to random gradient errors in standard quadrupoles of the lattice, correction quadrupoles are added at a location close to the standard quadrupoles. The correction quadrupoles are capable of varying the tune of the Tevatron by ± 1 tune unit at 900 GeV to keep a particle distribution in a "resonance-free" region of tune space.

Thus far, single particle motion in a synchrotron has been discussed for particle trajectories with a design energy specified by the magnitudes of the design magnetic fields. However, particle distributions in a synchrotron do not all have the design energy. If a particle is injected into the accelerator with an energy which does not match the accelerator's design energy, for example, a particle's energy will oscillate about the design energy. These energy oscillations, referred to as synchrotron oscillations, will couple into the particle's transverse motion through dispersion. Off momentum particles will no longer pass axially through the center of a quadrupole and consequently be subject to a focusing force. The closed orbit will thus be displaced from the central design orbit.[11] A particle's transverse position with a momentum offset is given by

$$x(s) = x_\beta(s) + \eta(s)\frac{\Delta p}{p_0}. \tag{2.26}$$

The free betatron oscillations of Equation 2.9 are denoted by $x_\beta(s)$. The momentum offset, Δp, is the measured deviation of the particle's momentum from the design momentum, p_0. The parameter $\eta(s)$ is called the dispersion and is in units of meters. Since orbits of higher momentum are usually at a larger radius in a high energy accelerator (when a particle's energy is above transition energy), the dispersion function is usually a positive function. In an accelerator which bends horizontally and thus lies in the horizontal plane, path length deviations from the design will occur horizontally. The dispersion function, therefore, is generally a non-zero function only in the horizontal plane. In the Tevatron, the horizontal dispersion in the arcs ranges from 2 to 6 meters. The rms momentum spread of a bunch distribution at 900 GeV is typically $\frac{\sigma_p}{p} = 0.0001$.

The dispersion $\eta(s)$ and the slope of the dispersion $\eta'(s) = \partial\eta(s)/\partial s$ are both Twiss parameters. Along with $\beta(s)$, $\alpha(s)$, and $\psi(s)$, they define a complete set of accelerator lattice parameters used to map a particle's linear motion in a synchrotron.

Given the dispersion and beta function at a specific location in the ring, the rms transverse size of a bunch distribution of emittance ϵ and momentum spread σ_p/p is completely defined. An unnormalized beam emittance defined at 1σ ($f = 0.15$ in Equation 2.20) gives an rms transverse beam size of

$$\sigma_i(s) = \sqrt{\beta_i(s)\ \epsilon_i + \left(\eta_i(s)\frac{\sigma_p}{p}\right)^2}. \tag{2.27}$$

The index i is used to emphasize the parameters which are defined in both transverse planes;

$i \equiv \hat{x}, \hat{y}$. Using the Fermilab definition of beam emittance (Equation 2.21), the rms transverse beam size in terms of normalized beam emittance is

$$\sigma_i(s) = \sqrt{\frac{\beta_i(s)\ \epsilon_{Ni}}{6\pi(\beta\gamma)_{rel}} + \left(\eta_i(s)\frac{\sigma_p}{p}\right)^2}. \tag{2.28}$$

Consider the variation of the rms transverse beam size in the arcs of the Tevatron at 900 GeV for a beam with a normalized emittance of 20π mm-mrad. A beta of 100 m and a dispersion of 6 m corresponds to a σ of 0.67 mm. A beta of 30 m and a dispersion of 2 m corresponds to a σ of 0.37 mm. A particle at 3σ in a particle distribution would occupy up to 2 mm in both transverse dimensions, or approximately 3 square mm in transverse space.

Because a spread of momentum exists in a particle distribution, particles will traverse a quadrupole magnet at different transverse positions. Consider a particle with its momentum expressed in terms of the design momentum and a momentum offset as $p = p_0(1 + \frac{\Delta p}{p_0})$. Upon traversing a focusing quadrupole of length L, the particle will see a change in the focal length of the quadrupole. The focal length of a quadrupole was previously found to be proportional to a particle's momentum; $f = p/(eB'L)$. By substituting the new momentum of the particle into this focal length expression, the change in focal length is found to be

$$\Delta f = \left(\frac{B\rho}{B'L}\right)\frac{\Delta p}{p}. \tag{2.29}$$

A positive momentum offset corresponds to a larger focal length. A particle with a positive momentum offset will thus be focused less than a particle at the design momentum. This leads to a chromatic focusing effect on a distribution of particles similar to chromatic effects seen in optical systems. A parameter called the chromaticity, ξ, is used to relate a particle's momentum offset to a corresponding change in its tune;

$$\Delta Q = \xi\ \frac{\Delta p}{p_0}. \tag{2.30}$$

The chromaticity is defined in each transverse plane of motion. By using the expression for the tune shift due to a quadrupole kick as described by Equation 2.25, the chromaticity is formally defined as

$$\xi = -\frac{1}{4\pi}\oint \beta(s)K(s)ds, \tag{2.31}$$

where $K(s)$ is the focusing strength of the lattice quadrupoles.[11] The natural chromaticity is the chromaticity of a synchrotron with no correction elements added to the lattice. The

natural chromaticity is approximately equal in magnitude and opposite in sign to the tune of the synchrotron.

Given a momentum spread in a particle distribution, a large chromaticity may cause a tune spread which is large enough that some of the particles have tunes that lie on or near undesirable resonances. To compensate for this effect, sextupole magnets are added as correction elements in the lattice. The magnetic field in a sextupole is quadratic in position; $B_x = \frac{1}{2}B'_x y^2$ and $B_y = \frac{1}{2}B'_y x^2$. Sextupole magnets, therefore, provide a field gradient which is linearly proportional to a particle's position offset. Using Equation 2.31, the contribution to the chromaticity from N sextupoles in the accelerator ring is

$$\xi_x = \frac{1}{2\pi}\sum_{i=1}^{N}\beta_x(s_i)\eta_x(s_i)k_x(s_i) \qquad \xi_y = \frac{1}{2\pi}\sum_{i=1}^{N}\beta_y(s_i)\eta_x(s_i)k_y(s_i) \tag{2.32}$$

where $k(s) = B''(s)L/B\rho$. The natural chromaticity is thus corrected for with the addition of sextupoles at high dispersion points in the ring. Note, however, that along with the beneficial contribution to the chromaticity, sextupoles do add nonlinearities to the lattice which must be accounted for to ensure stable running conditions.

2.2 Resonant Motion due to Magnetic Field Errors

Magnetic field errors arise from many sources in a real accelerator. There may be small magnet-to-magnet variations in the magnetic field produced even when the electric currents are the same in all magnets. Even if the magnetic field is within the design specifications, a magnet may be misaligned from its design position. This misalignment may occur in its transverse placement in the ring causing the particle to see field errors in normal components of the magnetic field. The misalignment may also manifest itself as a slight rotation of the magnet causing the particle to interact with skew components of the magnetic field. Magnetic fields along with field errors in a magnet are fully expressed as a fraction of the dipole bending field B_0 by[14],[13]

$$iB_x(x,y) + B_y(x,y) = B_0\sum_{n=0}^{\infty}(b_n + ia_n)(x+iy)^n. \tag{2.33}$$

The constants b_n and a_n are the multipole coefficients of the magnetic field.

Suppose that there is a constant magnetic field error in either a dipole or quadrupole which is located at $s = 0$. As discussed in Section 2.1 of this chapter, a particle's trajectory will be a free betatron oscillation about the unperturbed closed orbit. When the particle arrives at $s = 0$, the slope of its trajectory will change by an amount $\Delta\theta$. To constrain the

particle's motion to a new closed orbit, the trajectory of the orbit must close upon itself after one revolution.

$$x_c(s + 2\pi R) = x_c(s) \tag{2.34}$$

This constraint allows a closed orbit position to be calculated:

$$x_c(s) = \frac{\Delta\theta\sqrt{\beta(s)\beta_0}}{2\sin\pi Q}\cos(\Delta\psi - \pi Q) \tag{2.35}$$

where $0 < \Delta\psi < 2\pi$ and β_0 is the beta function at the location of the field error.[15] The displacement of the orbit is directly proportional to the magnitude of $\Delta\theta$ and the beta function at the location of the error. A resonant condition due to the field error is seen in the denominator of the closed orbit expression. As the tune approaches an integer, the amplitude of the oscillation will become large. This condition to be avoided is known as an integer resonance condition.

For completeness, let the transverse position of a particle be written explicitly as the sum of free betatron oscillations, energy oscillations and oscillations due to closed orbit errors. A subscript notation is used to denote $x_\beta(s)$ as the free oscillations of Equation 2.9 about the closed orbit given by Equation 2.35. The position $x_d(s)$ denotes the change in position due to dispersion effects as described in Equation 2.26. Beam position monitors in the accelerator will thus measure orbit positions which include all of these effects:

$$x(s) = x_\beta(s) + x_d(s) + x_c(s). \tag{2.36}$$

If a field error exists which is a quadrupole field error, the beta function in the accelerator will change. The deviation of the beta function from the beta function of the lattice design which is free from magnetic field errors is commonly referred to as a beta wave. The results of the derivation of a beta wave due to a small gradient error in a quadrupole is[15]

$$\frac{\Delta\beta(s)}{\beta(s)} = \frac{1}{2\sin 2\pi Q}\oint q(s')\beta(s')\cos 2(\Delta\psi - \pi Q)ds'. \tag{2.37}$$

The beta function of the real lattice normalized to the beta function of the design lattice is denoted by $\frac{\Delta\beta}{\beta}$. The parameter $q(s)$ is the quadrupole strength associated with the kick of magnitude $\Delta\theta$ a particle sees at a transverse position x: $qx = \Delta\theta$. Note that the denominator of the beta wave indicates a new set of resonances which must be avoided when quadrupole field errors are present. Half-integer values of the tune correspond to a beta wave of infinite magnitude. Along with an integer resonance, therefore, operating close to a half-integer resonance in an accelerator is a particularly dangerous condition. Regardless of whether

the particles are initially at a high oscillation amplitude or are in the core of the distribution, particles will grow in amplitude without bound and eventually be lost.

In general, if a magnetic field error exists in an accelerator, the transverse equation of motion of a particle becomes inhomogeneous:

$$\frac{\partial^2 x}{\partial s^2} + K(s)x = g(x,s). \tag{2.38}$$

The driving function, $g(x,s)$, is a force term which may be a nonlinear function of amplitude x and azimuth s.

A Courant-Snyder coordinate transformation into the normalized coordinates of Equation 2.18 along with a phase transformation will enable this inhomogenous Hill's equation to be expressed as the equation of motion of a driven harmonic oscillator. By reducing the phase $\psi(s)$ by Q such that $\phi(s) = \frac{1}{Q}\,\psi(s)$, the equation of motion becomes

$$\frac{\partial^2 x_N}{\partial \phi^2} + Q^2 x_N = -Q^2\,\beta^{\frac{3}{2}}(\phi)\,g(x_N,\phi). \tag{2.39}$$

The phase ϕ now advances by 2π after each turn. In the (x_N,ϕ) coordinates, the mathematical methods used to describe the motion of a driven harmonic oscillator become available. The notion of a resonance between a particle's tune and a harmonic amplitude of the driving term is the same as that of a simple harmonic oscillator.

The driving force is expressed in terms of m multipole moments of the dipole field error using Equation 2.33. A magnetic field expressed in terms of normal multipoles (assuming skew multipoles terms are equal to zero) in one dimension is given by

$$g(x_N,\phi) = \frac{\Delta B}{(B\rho)} = \frac{1}{(B\rho)}[\beta^{\frac{3}{2}}\,b_0 + \beta^{\frac{4}{2}}\,b_1 x_N + \beta^{\frac{5}{2}}\,b_2 x_N^2 + ... + \beta^{\frac{(m+3)}{2}}\,b_m x_N^m]. \tag{2.40}$$

The first, second and third terms denote the dipole, quadrupole and sextupole moments of the field error ΔB, respectively. In general, the mth term denotes the mth order multipole moment of the field error. Each multipole moment can drive a particle into resonance if the resonant frequency of the driving term equals that of the frequency of the solution to the homogeneous Hill's equation;

$$x_N(\phi) = A\cos(Q\phi + \delta). \tag{2.41}$$

Consider, for example, the resonance effects of a sextupole moment. The equation of motion expressed in terms of the b_2 moment is

$$\frac{\partial^2 x_N}{\partial \phi^2} + Q^2 x_N = -\frac{Q^2 B_0}{(B\rho)} \beta^{\frac{5}{2}}(\phi)\, b_2\, x_N^2. \tag{2.42}$$

If the driving term on the right hand side of the equation has the same frequency as a particle's tune, a resonant condition will exist. The right hand side is a product of a sextupole moment and x_N^2, both of which can be alternatively expressed as Fourier series in ϕ. The frequency of the driving term is a combination of the frequency $2Q$ expressed by x_N^2 and the harmonic frequency of $b_2\beta^{\frac{5}{2}}$. If the product $b_2\beta^{\frac{5}{2}}$ has a nonvanishing pth harmonic such that $p \pm 2Q = Q$, a resonant condition exists. The frequency $p + 2Q = Q$ leads to the condition that the tune should not be an integer if one wants to avoid a resonant condition. The frequency $p - 2Q = Q$ leads to the condition that the tune should not be a third of an integer.[9]

In general, the equation of motion for a driven harmonic oscillator is well suited for discussion using Hamiltonian techniques. Chapter 3 will concentrate on the Hamiltonian approach to solving this equation of motion for the nonlinear driving force of the beam-beam interaction.

2.3 THE TEVATRON AS A COLLIDER

In a typical colliding beam store, six proton bunches and six antiproton bunches circulate in the Tevatron in opposite directions. A given proton bunch passes by an opposing antiproton bunch at twelve locations in the ring. The details of the electromagnetic beam-beam interaction which occur at these twelve crossing points will be reviewed in the next chapter, so suffice it to say here that the beam-beam interaction will cause a tune spread of particles in the distribution which may cause some particles to shift onto resonances.

It was experimentally determined, for example, in the first Tevatron Collider Run (1987-1988) that the dominant factor limiting the luminosity was the beam-beam interaction. A "beam-beam limit" was reached in the Collider; the luminosity could not be increased by decreasing the beam emittance or by increasing the bunch intensity of the protons.[2] In order to minimize the adverse effects of the beam-beam interaction, electrostatic separators were installed in the Tevatron. The separators are oppositely charged stainless steel parallel plates which provide a transverse electrostatic field in the path of the particle. The electrostatic field causes particles of opposite charge to circulate on different closed orbits. The electrostatic fields in the Tevatron are in both transverse dimensions, causing closed orbits of the protons and antiprotons to wrap around each other in a double-helical fashion.

This ability to separate the beams in two dimensions is a unique capability of the Tevatron Collider. It proved to be a successful method of limiting adverse effects of the beam-beam interaction during normal collider operation.

The separators are configured to separate the beams everywhere except at the location of the Colliding Detector Facility (CDF) detector located at the B0 straight section and at the D0 detector. In order to provide the highest luminosity at these locations, 'low-beta' insertions are added.[5] Low beta insertions are composed of quadrupoles of a much larger focusing gradient than the quadrupoles used for focusing in the arcs. A low beta quadrupole in the Tevatron, for example, has twice the focusing gradient of a standard quadrupole, operating with a magnetic field gradient of 140 T/m at 1 TeV. Low beta quadrupoles are also much longer than quadrupoles in the arcs (approximately 180 inches as compared to 66 inches for a standard quadrupole) and thus have more than six times the focusing strength.

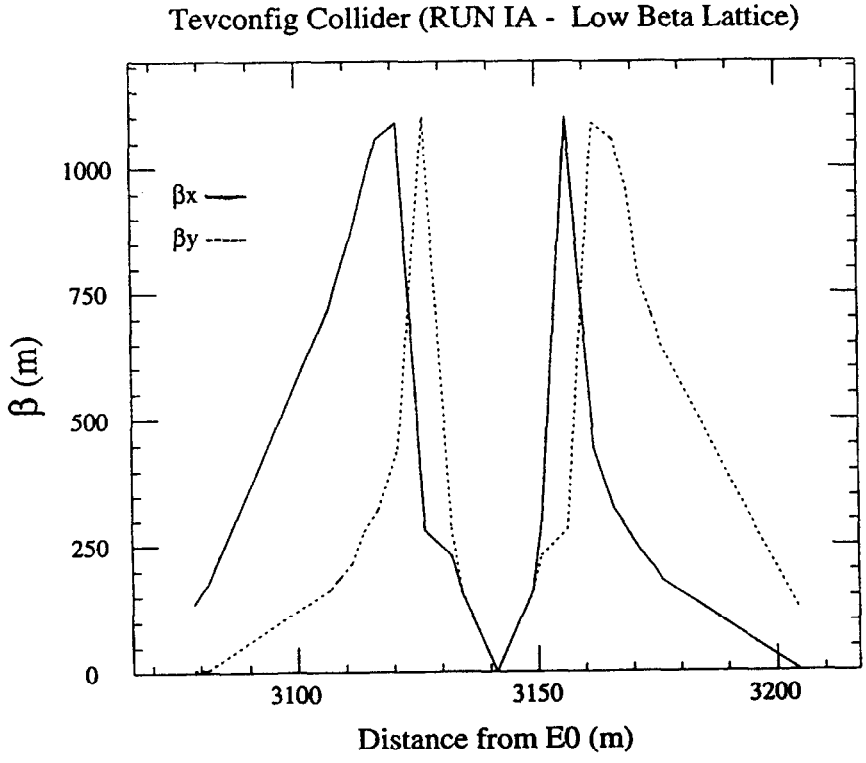

Figure 2.6: The horizontal (solid line) and vertical (dashed line) beta function at the CDF interaction region as specified by the design lattice of Collider Run IA.

The advantage of greater focusing strength is seen by substituting the transverse rms beam size of Equation 2.21 into the luminosity expression of Equation 1.2.

$$L = \frac{3 f_{rev} N_p N_{\bar{p}}}{2\beta\epsilon} F(z) \tag{2.43}$$

For a given emittance and bunch intensity, the highest luminosity will be achieved at the lowest beta. The strong focusing properties of the low beta insertion reduces the magnitude of the beta function at the collision point to less than a meter. The result of such strong focusing is that a transverse rms bunch size of approximately 1 mm in the arcs is focused to approximately 30 microns at the detector locations.

It is of interest to examine the change in the beta function in a low-beta insertion. The beta function through a straight section is found by setting the focusing strength equal to zero in Equation 2.11 and solving for β.

$$K = 0: \quad \beta(s) = \beta^* - 2\alpha^* s + \frac{(1+\alpha^*)^2}{\beta^*} s^2 \tag{2.44}$$

The lattice parameters denoted by the asterick are defined at the collision point which is, by definition, located at the azimuthal location $s = 0$. During Collider Run IA, the beta function varied quadratically from approximately 0.35 meters at either the B0 or D0 interaction points to 130 meters at the quadrupoles which marked the endpoints of the B0 and D0 straight sections. The variation of the beta function in the B0 interaction region as calculated from a model of the Tevatron is shown in Figure 2.6. The highest beta in the Tevatron (approximately 1100 meters) is reached at the defocusing low beta quadrupole locations in the low beta insertion.

2.4 Accelerator Parameters during Collider Runs IA and IB

Collider Run IA (1992-1993) and Collider Run IB (1994-1995) are characterized by operational accelerator parameters which are quite similar. An increase in the luminosity is apparent in Collider Run IB as the bunch intensities increase and operation of the accelerator continues to improve.

Collider Run IA was split into two "low-beta modes" of operation in which the magnitude of beta at both head-on collision points was changed. The first part of the run intended to collide protons and antiprotons at the B0 and D0 collision points with a 0.5m value of β^*. The presence of a beta wave in the Tevatron resulted in a lower β^* than the design value at both the B0 and D0 interaction points. The existence and consequences of the beta wave are discussed in the latter part of this section. The second part of the collider run attempted

to lower β^* to 0.25m to further increase the luminosity.

At the time of this writing, Collider Run IB has operated exclusively with a β^* of approximately 0.35m. Current machine studies are testing the possibility of operating at a β^* of 0.25m in the latter part of Run IB.

The experimental measurements which are presented in this dissertation were taken using the 0.5m β^* lattice of Collider Run IA and the 0.35m β^* lattice of Collider Run IB. Consequently, the conditions of operation discussed here concern only those relevant parts of Run IA and Run IB. Typical values of operational accelerator parameters during Collider Run IA and Collider Run IB are listed in Table 2.1.

Tevatron Accelerator Parameters

Parameter	**Symbol**	**Run IA**	**Run IB**
Kinetic Energy	E (GeV)	900	900
Dipole Bend Radius	ρ (m)	754	754
Revolution Frequency	f_{rev} (kHz)	47.7	47.7
Magnetic Rigidity	$\|B\rho\|$ (T-m)	3×10^3	3×10^3
Horizontal Tune	Q_x	20.585	20.583
Vertical Tune	Q_y	20.575	20.575
Synchrotron Tune	Q_s	5.7×10^{-4}	5.7×10^{-4}
Momentum Spread	σ_p/p	1×10^{-4}	1×10^{-4}
Protons per bunch	N_p	120×10^9	200×10^9
Antiprotons per bunch	$N_{\bar{p}}$	40×10^9	70×10^9
Proton Transverse Emittance	ϵ_{N_p} (π mm-mrad)	25	25
Antiproton Transverse Emittance	$\epsilon_{N_{\bar{p}}}$(π mm-mrad)	15	15
Longitudinal Emittance	ϵ_l (eV-sec)	4	4

Table 2.1: Tevatron accelerator parameters in Collider Run IA and Collider Run IB.

The actual collider lattice in the 0.5m β^* part of Run IA differed from its intended design in that a beta wave existed in both transverse dimensions of the Tevatron. As shown in Equation 2.37, a small perturbation of the strength of a quadrupole from its design specification will produce a beta wave which modifies the beta function of the design lattice. The problem in the Tevatron occurred in the magnetic fields produced by the quadrupoles in the low beta insertions. The transfer constants which represent the actual field produced for a given current differed in the real accelerator from the design specifications. The difference

between the beta function as specified by the design lattice and the beta function which was actually present during Collider Run IA is shown for a section of the Tevatron in Figure 2.7.[19]

The perturbation of the strength of the low beta quadrupole is too large to be described exactly by Equation 2.37. A perturbative analysis is not valid in this case.[20] It should be noted that the beta wave was corrected for in Collider Run IB by adding "low-beta trims"; power supplies were installed which allowed independent control of upstream and downstream low-beta quadrupoles to compensate for the gradient errors.

Tevatron Lattice Parameters

Lattice Parameter	**Symbol** (units)	**Run IA**		**Run IB**	
		B0	D0	B0	D0
Horizontal beta	β_x (m)	0.39	0.49	0.35	0.35
Vertical beta	β_y (m)	0.41	0.44	0.33	0.34
Horizontal dispersion	η_x (m)	0.02	0.01	-.005	0
Slope of dispersion	η_x'	0.08	0.06	0.28	0.28
Horizontal alpha	α_x	-0.34	-0.57	0.01	0.01
Vertical alpha	α_y	0.16	0.23	0.02	0.01

Table 2.2: Tevatron lattice parameters in Collider Run IA and Collider Run IB.

As Equation 2.37 indicates, a beta wave is directly proportional to the beta function at the location of the field error. The magnetic field error which produced the beta wave in the Tevatron occurred in a low beta quad which is at a high beta location. Peaks in the resulting beta wave were approximately 50% greater than that of the design during the 0.5m β^* run. Note, though, that the value of the beta function at the two head-on collision sites was lower than the design value. This was a nice consequence of the beta wave. The measured luminosity obtained during the 0.5m β^* run was greater than what was estimated using the design lattice.

Lattice parameters at the B0 and D0 interaction points for the 0.5 m β^* lattice of Collider Run IA and the 0.35 m β^* lattice of Collider Run IB are listed in Table 2.2.

The beta wave did cause some problems in operation though. When changing the tune in the Tevatron, it was found that the measured chromaticity also changed. Experiments which will be discussed in Chapter 5 indicated that the change in the measured chromaticity per tune unit using the 0.5m β^* lattice was approximately

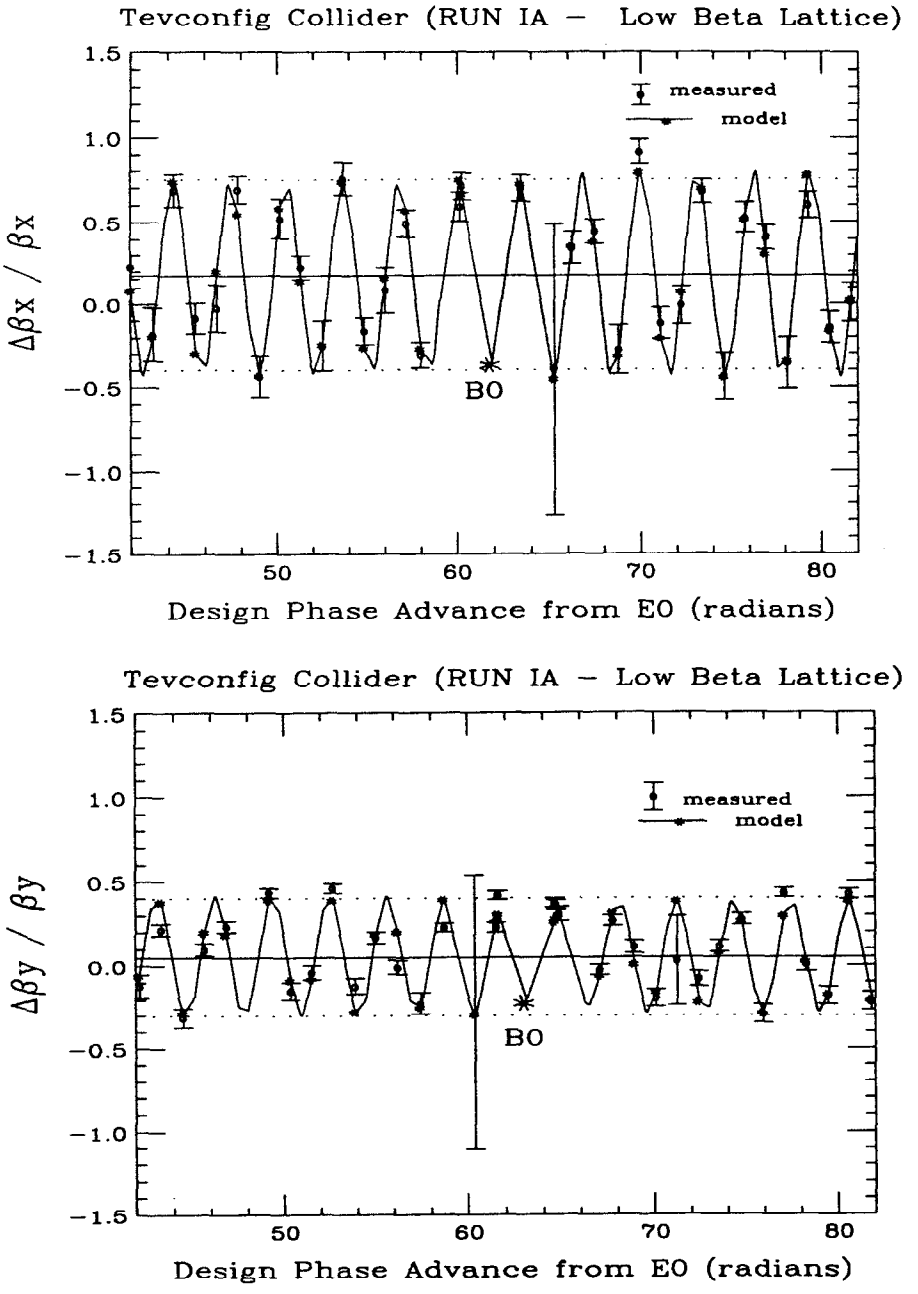

Figure 2.7: The horizontal and vertical beta wave in a section of the Tevatron. The vertical axis is the variation of beta from the design lattice. The solid line connects points calculated from a model of the Tevatron (Tevconfig) for Collider Run IA. Actual measurements of the beta function occurred at the points denoted by circles with error bars.

$$\frac{\Delta\xi_x}{\Delta Q_x} = 117 \quad \frac{\Delta\xi_y}{\Delta Q_y} = 50. \tag{2.45}$$

To verify this dependence of the 0.5m β^* lattice on the tune, the change in chromaticity per change in tune was calculated for two different models of the Tevatron. One of the models of the Tevatron contained the design lattice only and the other lattice more closely reproduced the beta wave in the Tevatron. The chromaticity did not vary when changing the tune of the design lattice. The chromaticity did change, however, when it was calculated for different tune settings of the lattice describing the beta wave. The calculated results showed good agreement with the experimental results. The reason for the change in chromaticity in the lattice describing the beta wave could be seen in the beta function. The average beta around the ring did not vary largely when the tune was changed in the design lattice, but there was a large increase in the average beta around the ring when the tune was changed in the lattice describing the beta wave.[17] As indicated in Equation 2.32, if there is an increase in the average beta around the ring, the chromaticity will increase also.

Chapter 3

THE BEAM-BEAM INTERACTION

3.1 THE BEAM-BEAM FORCE

A weak-strong model of the beam-beam interaction is used to define the motion of a "weak" or low intensity bunch colliding with a "strong" or high intensity bunch. A weak-strong picture of the beam-beam interaction translates in the Tevatron to an antiproton bunch colliding with a static electromagnetic field generated by a round, Gaussian, and short proton bunch. Antiprotons, in a weak-strong model, are the main focus of attention as test particles. Test particles differ from each other in that they have different amplitudes (a_x, a_y, a_s). The proton intensity is assumed to be large enough that protons are unaffected by the weak electromagnetic fields generated by low intensity antiprotons.

In the first approximation, the angular deflection a single antiproton experiences as it collides with a proton charge distribution does not depend on the longitudinal charge distribution of the protons.[28] The transverse charge distribution is assumed Gaussian and round for the counter-rotating proton bunch. In cylindrical coordinates, the proton charge distribution is given by

$$\rho(r) = \frac{ne}{2\pi\sigma^2} \exp\left[-\frac{r^2}{2\sigma^2}\right], \tag{3.1}$$

where σ is the rms transverse size of the bunch, n is the number of protons per unit length and e is the proton charge.

The electromagnetic force an antiproton experiences as it traverses a proton bunch is described by the Lorentz force:

$$\vec{F} = e(\vec{E} + \vec{v} \times \vec{B}) = e(E_r \pm \beta_{rel} c B_\phi)\, \hat{r}, \tag{3.2}$$

where $\hat{r}$ is a radial unit vector. A positive sign of the magnetic force term represents the force due to electromagnetic interactions with colliding protons; the beam-beam force. A negative magnetic force term corresponds to the Coulomb force between antiprotons in the same bunch; intrabeam scattering. The electric and magnetic fields counteract each other in the case of intrabeam scattering, but are additive in the case of the beam-beam force.

The electric field, E_r, and the magnetic field B_ϕ are described by Gauss' theorem and Ampere's Law, respectively.

$$E_r = \frac{ne}{2\pi\epsilon_0}\frac{1}{r}\left(1 - e^{-\frac{r^2}{2\sigma^2}}\right) \tag{3.3}$$

$$B_\phi = \frac{ne\mu_0\beta_{rel}\,c}{2\pi}\frac{1}{r}\left(1 - e^{-\frac{r^2}{2\sigma^2}}\right) \tag{3.4}$$

The kick $\Delta r'$ an antiproton receives from an interaction force F_r is

$$\Delta r' = \frac{L}{2\beta_{rel}c}\frac{1}{e(B\rho)}F_r, \tag{3.5}$$

where L is the proton bunch length. The beam-beam kick is found by substituting the beam-beam force into the kick expression:

$$\Delta r' = -\frac{2Nr_p}{\gamma_{rel}}\frac{1}{r}\left[1 - \exp\left(-r^2/2\sigma^2\right)\right]. \tag{3.6}$$

The classical radius of the proton is denoted by r_p and N is the total number of protons in the bunch ($N = nL$). Equation 3.6 is the beam-beam kick for a "head-on" beam-beam collision; the antiproton is oscillating about the same closed orbit as the centroid of the opposing proton bunch.

Figure 3.1 describes the beam-beam kick as a function of the oscillation amplitude of an antiproton normalized to σ of the opposing proton distribution. If the antiproton collides at a normalized amplitude which is much less than one, the kick is linear in r. The particle experiences an "electrostatic lens" force which, unlike a magnetic quadrupole, focuses in both the horizontal and vertical directions. When the normalized amplitude is approximately equal to one, the force on the antiproton becomes highly nonlinear. As shown in the figure, the beam-beam kick decreases like $1/r$ at large amplitudes.

For a small amplitude particle in one dimension, $x = r \ll \sigma$ and the beam-beam kick acts like a thin lens of focal length f, where

$$\frac{1}{f} = \frac{\Delta x'}{x}. \tag{3.7}$$

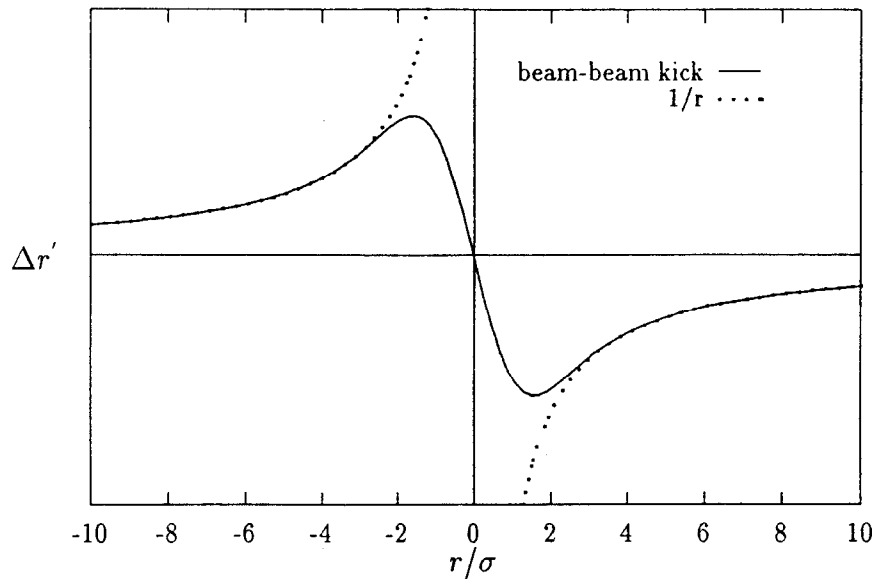

Figure 3.1: Angular deflection due to a proton-antiproton electromagnetic interaction as a function of the oscillation amplitude of a particle. The oscillation amplitude is normalized to the rms σ of the opposing charge distribution. A $1/r$ asymptotic dependence is observed.

Substituting for the focal length in Equation 2.25 (remembering $q = 1/f$), the tune shift of a small amplitude particle due to the beam-beam kick is

$$\begin{aligned} \xi &\simeq \frac{1}{4\pi}\beta\frac{\Delta x'}{x} \\ &= \frac{Nr_p\beta}{4\pi\gamma_{rel}\sigma^2}, \end{aligned} \tag{3.8}$$

where β is measured at the beam-beam crossing point. The beam-beam tuneshift parameter ξ is an important scale factor which parameterizes the strength of the beam-beam kick. For non-round beams, the beam-beam tuneshift parameter is[28]

$$\xi_{x,y} = \frac{Nr_0\beta_{x,y}}{2\pi\gamma_{rel}\sigma_{x,y}(\sigma_x+\sigma_y)}. \tag{3.9}$$

3.2 A Hamiltonian Analysis

A two-dimensional Hamiltonian of a weak-strong colliding beam system is defined as

$$H(x,p_x,y,p_y;s) = \frac{1}{2}(p_x^2+K_xx^2)+\frac{1}{2}(p_y^2+K_yy^2)+V(x,y)\sum_{l=-\infty}^{\infty}\delta[s-(2\pi Rl)] \tag{3.10}$$

where p_x and p_y are the canonical momenta associated with a particle's transverse positions in the horizontal and vertical planes, respectively.[32][24] The summation over l is a summation of the periodic crossing points in which a particle receives a localized beam-beam kick.

The beam-beam potential is described by Poisson's equation $\nabla^2 V = -\rho/\epsilon_0$ with the constraint that $V \to 0$ as $x, y \to \infty$.[33] In terms of x and y, the transverse charge distribution of Equation 3.1 is rewritten:

$$\rho(x,y) = \frac{ne}{2\pi\sigma_x\sigma_y} \exp\left[-\frac{1}{2}\left(\frac{x^2}{{\sigma_x}^2} + \frac{y^2}{{\sigma_y}^2}\right)\right]. \tag{3.11}$$

The beam-beam potential due to this charge distribution is

$$V(x,y) = \frac{Nr_p}{\gamma_{rel}} \int_0^\infty dt \, \frac{1 - \exp\left[-\frac{x^2}{2\sigma_x^2+t} - \frac{y^2}{2\sigma_y^2+t}\right]}{\sqrt{2\sigma_x^2+t}\sqrt{2\sigma_y^2+t}}. \tag{3.12}$$

An integration over the bunch length has occurred in the above expression, as evidenced by a change in the particles per unit length n to the total particles in the distribution N.

The symmetry of the potential expression dictates that only even-ordered resonances will be driven in head-on collisions. An expansion of the exponential term in the potential gives terms of order $x^{2n}y^{2m}$, where n and m are integers. In other words, $|n_x| \pm |n_y|$ of Equation 2.24 must be equal to an even integer. Just like any nonlinear resonance driving term (caused by sextupole magnets or octupole magnets, for example), these driving terms excite resonances whenever the betatron tunes satisfy the resonance condition described by Equation 2.24.

Odd-ordered resonances require the symmetry of the potential to be broken, and are present when the beams are separated transversely or when there is dispersion or a crossing angle at the collision point. If there is a transverse separation between the closed orbit of the particle and the centroid of the colliding particle distribution, the potential is redefined as

$$V(x,y) = \frac{Nr_p}{\gamma_{rel}} \int_0^\infty dt \, \frac{1 - \exp\left[-\frac{(x-d_x)^2}{2\sigma_x^2+t} - \frac{(y-d_y)^2}{2\sigma_y^2+t}\right]}{\sqrt{2\sigma_x^2+t}\sqrt{2\sigma_y^2+t}}, \tag{3.13}$$

where d_x and d_y denote the horizontal and vertical separations of a particle from the centroid of the bunch distribution.

At a single crossing point, the equations of motion described by the Hamiltonian of Equation 3.10 are

$$\frac{dz^2}{ds^2} + K_z(z) = -\frac{\partial V}{\partial z}\,\delta[s],\quad z \equiv x, y. \tag{3.14}$$

THE UNPERTURBED HAMILTONIAN

Consider the simple case of a one-dimensional system ($y = 0$) in which the beam-beam potential is equal to zero. Hamilton's equation $\partial H/\partial p_x = x'$ yields the relation $p_x = x'$ and confirms the conjugate coordinate of the position x as x'. A generating function is used to canonically transform the Hamiltonian into a new Hamiltonian using action-angle coordinates $(\vec{J}, \vec{\phi})$. The new Hamiltonian has the advantage of being independent of the longitudinal coordinate s if one introduces a periodic coordinate, $\tilde{\psi}_x$, which is related to ψ_x of Equation 2.12 by

$$\tilde{\psi}_x = \psi_x - Q_x\theta = \psi_x - \frac{Q_x s}{R}. \tag{3.15}$$

The generating function used in the canonical transformation is given by[31]

$$\begin{aligned} G_x(x, \phi_x; s) &= -\frac{x^2}{2\beta_x}[\tan F_x + \alpha_x], \quad where \\ F_x &\equiv \psi_x - Q_x\theta + \phi_x \end{aligned} \tag{3.16}$$

This generating function produces the coordinate transformations[21]

$$x = \sqrt{2J_x\beta_x}\cos(\tilde{\psi}_x + \phi_x) \tag{3.17}$$

$$x' = -\sqrt{\frac{2J_x}{\beta_x}}\left[\sin(\tilde{\psi}_x + \varphi_x) + \alpha_x\cos(\tilde{\psi}_x + \phi_x)\right], \tag{3.18}$$

and the new Hamiltonian is

$$H_1 = H(x, x'; s) + \frac{dG_x}{ds} = \frac{Q_x J_x}{R}. \tag{3.19}$$

The parameter R is a scaling of the longitudinal parameter s. By rescaling the Hamiltonian using θ, the parameter R is eliminated. Recalling that $d/d\theta = Rd/ds$, the Hamiltonian is

$$H_1(J_x, \phi_x; \theta) = H_1(J_x, \phi_x; s) \times R = Q_x J_x. \tag{3.20}$$

The equations of motion are given by

$$\dot{\phi}_x = \frac{\partial H_1}{\partial J_x} = Q_x, \tag{3.21}$$

$$\dot{J}_x = -\frac{\partial H_1}{\partial \phi_x} = 0, \tag{3.22}$$

where the dot notation designates a derivative with respect to θ. With no beam-beam interaction, the amplitude of a particle at a given location remains constant: $J_x = constant$. J_x is therefore equal to the area enclosed by the ellipse in (x, x') phase space. The invariant single particle emittance is closely related to the invariant J_x; $J = A^2/2$, where πA^2 is the invariant described in Equation 2.17.

An equivalent derivation holds for both transverse degrees of freedom. The unperturbed part of the Hamiltonian described by Equation 3.10 is thus

$$H(\vec{J}, \vec{\phi}; \theta) = Q_x J_x + Q_y J_y = \vec{Q} \cdot \vec{J} \tag{3.23}$$

This system is equivalent to a system of two uncoupled harmonic oscillators.

THE RESONANT HAMILTONIAN

It is of interest to examine a particle's motion due to a single resonance, that is, to isolate part of the Hamiltonian when a particle's tune Q is close to a value satisfying $nQ \approx p$, where n and p are integers. The resulting "resonant" Hamiltonian is used to delineate a particle's motion when its tune is close to a resonance of order n. With the inclusion of the beam-beam perturbation, the resonant Hamiltonian is of the form[32][24]

$$H_n(\vec{J}, \vec{\phi}; \theta) = \vec{Q} \cdot \vec{J} + \vec{\xi}\, U(\vec{J}) + \vec{\xi} V_n(\vec{J}) \cos(\vec{n} \cdot \vec{\phi} + m\theta). \tag{3.24}$$

The first term in the Hamiltonian describes the linear motion of a particle near a resonance of order n. The last two terms are scaled by the linear beam-beam tuneshift parameter; both terms are due to the beam-beam interaction. The term $U(\vec{J})$ is the amplitude detuning function which describes the variation of tune with amplitude due to the beam-beam interaction. The term $V_n(\vec{J})$ is a beam-beam "resonant excitation" term and is known as the resonance width function.[32] Each of these terms will be discussed in more detail in the next two sections.

An important property of a single resonance model is found from Hamilton's equation of motion describing a particle's amplitude.[21] Motion dominated by a single resonance is given by

$$\dot{\vec{J}} = \vec{n}\ (\vec{\xi} V_n(\vec{J})\ \sin(\vec{n} \cdot \vec{\phi} + m\theta)\ ). \tag{3.25}$$

The dot denotes a derivative with respect to θ. Equation 3.25 points to a relation between the two transverse amplitudes:

$$\frac{\dot{J}_x}{n_x} + \frac{\dot{J}_y}{n_y} = constant \tag{3.26}$$

or, equivalently,

$$\frac{J_x}{n_x} + \frac{J_y}{n_y} = c_1 + c_2 f(\theta) \tag{3.27}$$

where c_1 and c_2 are constants. A particle's motion plotted in amplitude space (J_x, J_y) follows a straight line. Motion in amplitude space is bounded or unbounded depending upon the signs of n_x and n_y. Bounded motion occurs when one of the components of $\vec{n}$ are negative; when the resonance is a "difference resonance". A growth in a particle's horizontal amplitude, for example, will lead to a decrease in a particle's vertical amplitude. Unbounded growth in amplitude occurs when both components of $\vec{n}$ are positive; when the resonance is a "sum resonance". This relation has led to a popular assumption that sum resonances are dangerous resonances and that difference resonances are safe. What is not considered in this assumption is that even in the case of bounded motion in amplitude space, a particle still has the potential of being lost due to a large amplitude growth in one dimension.

3.3 THE BEAM-BEAM TUNE SHIFT

In the absence of all resonances ($n = 0$), a particle's tune shift due to the beam-beam interaction is derived from the amplitude detuning function $U(\vec{J})$ in the resonant Hamiltonian. This amplitude detuning function is obtained from the beam-beam potential using the action-angle coordinate transformation of Equation 3.15. In the case of round beams, $\sigma_x = \sigma_y$ is σ and the beam-beam potential in terms of action-angle coordinates is given by

$$V(\vec{J}, \vec{\phi}) = \frac{N r_o}{\gamma} \int_0^\infty dt \, \frac{1}{2\sigma^2 + t} \left(1 - \prod_{k=1,2} \exp \left[\frac{-\left(\sqrt{2J_k \beta_k} \cos \phi_k - d_k\right)^2}{2\sigma^2 + t} \right] \right). \tag{3.28}$$

The product over k represents the two transverse dimensions; $(1,2) \equiv (x,y)$.

Consider the case of a non-zero separation d in the horizontal direction. Equation 3.28 is rewritten as

$$V(\vec{J}, \vec{\phi}) = \frac{N r_o}{\gamma} \int_0^1 \frac{du}{u} \left(1 - \exp \left[-u \left(\sqrt{\frac{J_x}{2\epsilon}} \cos \phi_x - \frac{d_N}{2} \right)^2 - u \frac{J_y}{2\epsilon} \cos^2 \phi_y \right] \right). \tag{3.29}$$

The separation, d_N, is a normalized horizontal separation ($d_N \equiv d/\sigma$). The variable of integration has been changed to u, where $u \equiv 1/(1 + (t/\sigma^2))$. The beam emittance ϵ is substituted into the expression ($\epsilon = \sigma^2/\beta$), where the beam emittance of Equation 2.20 is defined at 1σ.

The detuning function of the resonant Hamiltonian is found by averaging the beam-beam potential over all angles. In one dimension, the detuning term in the resonant Hamiltonian is

$$\xi\, U(J) = \frac{1}{2\pi}\int_0^{2\pi} V(J,\phi)\, d\phi. \tag{3.30}$$

The beam-beam tune shift is obtained from the derivative of the detuning term. This is seen by examining Hamilton's phase equation of motion. In the absence of resonances,

$$\frac{d\phi}{d\theta} = \frac{\partial H}{\partial J} = Q - \xi\frac{\partial U(J)}{\partial J} \tag{3.31}$$

or, equivalently, the shift in tune is

$$\Delta Q = \xi\frac{\partial U(J)}{\partial J}. \tag{3.32}$$

Horizontal and vertical tune shifts for round beams in the presence of a non-zero horizontal separation are given by[29]

$$\frac{\Delta Q_x}{\xi_x} = \frac{1}{2\pi}\int_0^{2\pi} d\phi\, \frac{\cos\phi}{\alpha_x\left[\cos\phi - \frac{d_N}{2\sqrt{\alpha_x}}\right]}\left(1 - \exp\left[-2\left(\sqrt{\alpha_x}\cos\phi - \frac{d_N}{2}\right)^2\right]\right) \tag{3.33}$$

and

$$\frac{\Delta Q_y}{\xi_y} = \frac{1}{2\pi}\int_0^{2\pi} d\phi\, \frac{\cos^2\phi}{\alpha_y\cos^2\phi + \frac{d_N^2}{4}}\left(1 - \exp\left[-\left(2\alpha_y\cos^2\phi + \frac{d_N^2}{2}\right)\right]\right). \tag{3.34}$$

For convenience, the parameter α has been used in the above expressions, where

$$\alpha_k = \frac{J_k}{2\epsilon_k}, \tag{3.35}$$

and $k \equiv x, y$. Horizontal and vertical tune shifts for various beam separations in the horizontal plane are plotted in Figure 3.2. Tune shifts are plotted as a function of normalized particle amplitude, a. The amplitude of a particle is defined in terms of action-angle coordinates as

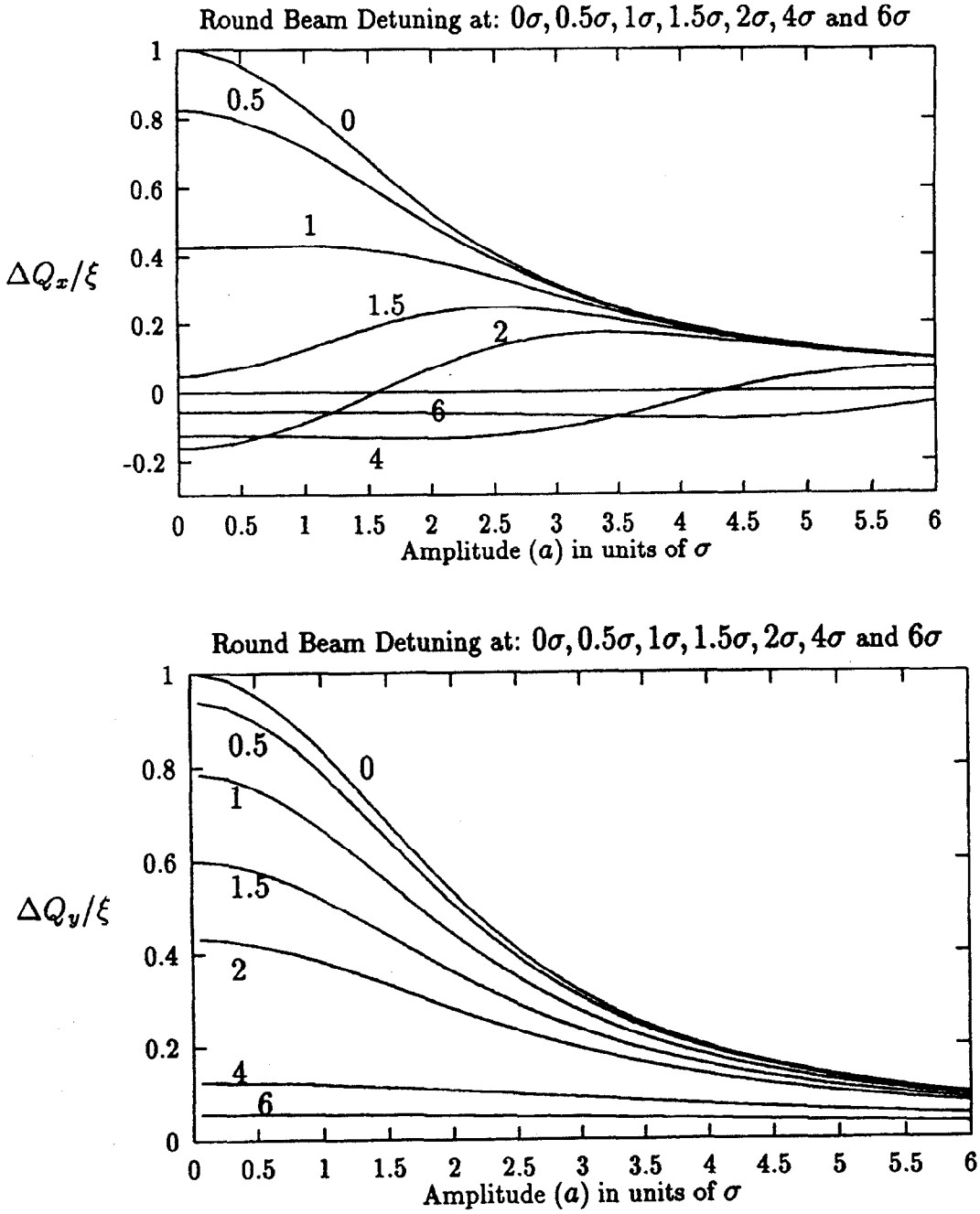

Figure 3.2: Horizontal and vertical tune shift due to beam-beam detuning in the presence of horizontal separation. A round beam approximation is used.

$$a = \sqrt{x^2 + (\alpha x + \beta x')^2} = \sqrt{2\beta J} \tag{3.36}$$

Normalizing to the transverse beam size of the proton distribution,

$$a = \sqrt{\frac{2J}{\epsilon}} \tag{3.37}$$

and is in units of σ.

Note that horizontal and vertical tune shifts are scaled by the beam-beam tuneshift parameter. Maximum tune shifts for any amplitude particle occur in the case of head-on collisions. In head-on collisions, small amplitude particles are shifted in tune by the largest amount. The shift in tune decreases nonlinearly with particle amplitude. Amplitude dependent tune shifts lead to a spread in particle tunes for a distribution of particles. The antiproton tune spread characteristic of one head-on collision in the Tevatron during Collider Run IB is mapped in Figure 3.3 as a "beam-beam tune footprint". In the figure, the tune which is unperturbed by the beam-beam interaction (referred to as the base tune in this work) is marked with a cross mark. Zero amplitude antiprotons are shifted linearly in tune by approximately 0.006 tune units both horizontally and vertically. A typical Collider Run in the Tevatron operates with two head-on collisions and thus with a linear tune shift ξ of 0.012.

The beam-beam interaction redefines the working point for particles with unperturbed tunes into a working area in tune space. For good beam lifetimes and stable operating conditions, it is desirable to keep the entire area in which particles are spread in tune away from destructive resonance lines in tune space.

It is interesting to note that the amplitude dependent tune shift which results from the beam-beam interaction is predicted to have a stabilizing effect on a particle in resonance. Consider a situation in which a small amplitude particle is driven into resonance and experiences amplitude growth. The tendency of the particle to take on different tunes as it grows in amplitude characterizes a "detuning" effect. The rate of a particle's amplitude growth will decrease as the particle is shifted in tune off of a resonance. The detuning effect brings the destructive effects of the resonance under control. This is an important aspect of the beam-beam force. The phase space of a particle in the presence of the beam-beam interaction is always a closed phase space; a chaotic region which may exist will not extend to infinity. Previous beam-beam studies have examined the onset of resonance islands in phase space and the overlap of resonance islands which leads to chaotic motion. Surprisingly, typical strengths of the beam-beam interaction in hadron colliders are much smaller than that predicted for the onset of chaotic motion in a particle's phase space. Resonance overlap

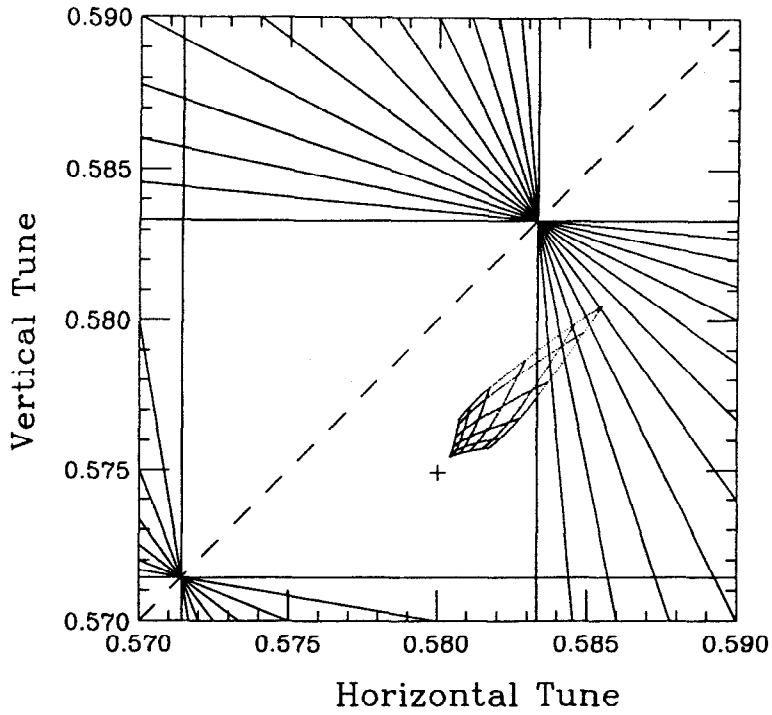

Figure 3.3: Beam-beam tune footprint for one head-on collision in the Tevatron Collider. The footprint was calculated analytically for antiprotons with oscillation amplitudes ranging from 0 to 5σ.

has been observed when an external modulation, such as a tune modulation, is added to the beam-beam model.[24][23][22]

In a real collider, though, beam stability in the presence of the beam-beam interaction is not observed. It will be shown in this work that higher background rates are driven by the beam-beam interaction in the Tevatron when the operating tune is near 7th and 9th order resonances. The SPS collider at the European Laboratory for Particle Physics (CERN) found destructive beam-beam effects (a decrease in beam lifetime) due to the 16th order resonance. Higher background rates were also measured in the SPS due to an increased beam-beam interaction effect for proton and antiproton emittances of unequal size.[26] A long range beam-beam experiment performed in the Tevatron collider showed an increased beam loss when the proton and antiproton bunches were separated by about 1.5 σ to 2.0 σ.[27]

3.4 AMPLITUDE OF A RESONANCE

As expressed in Equation 3.28, the beam-beam potential is an even function in angle. In one dimension, the Fourier series expansion of the beam-beam potential is

$$V(J,\phi) = \sum_{n=1}^{\infty} V_n(J)\cos n\phi, \tag{3.38}$$

where the summation over n includes all orders of resonances. In an isolated resonance model, a single resonance of order n is accepted as the dominant resonant term. Higher order terms are neglected as contributing to a particle's resonant motion. The resonant width function, $V_n(J)$ of Equation 3.24, represents the amplitude of the dominant resonant excitation term in the beam-beam potential.

The amplitude of a beam-beam resonant driving term is obtained from the derivative of the beam-beam potential ($\vec{F} = -\nabla V$). The Fourier series expansion of beam-beam driving terms of order n is given by

$$\left(\frac{\partial V(J,\phi)}{\partial J}\right) = \sum_{n=1}^{\infty}\left(\frac{\partial V_n(J)}{\partial J}\right)\cos n\phi. \tag{3.39}$$

The amplitude of a resonance of order n is the nth Fourier component of its Fourier series expansion. This amplitude is the derivative of the resonance width function with respect to J.

$$\left(\frac{\partial V_n(J)}{\partial J}\right) = \frac{1}{\pi}\int_0^{2\pi} d\phi\left(\frac{\partial V(J,\phi)}{\partial J}\right)\cos n\phi \tag{3.40}$$

Substituting the beam-beam potential of Equation 3.28 into the above expression gives the amplitude of a resonance due to the beam-beam interaction:

$$V_n'(\alpha) = \xi\frac{1}{2\pi}\int_0^{2\pi} d\phi\frac{\cos n\phi\cos\phi}{\alpha\left(\cos\phi - \frac{d_N}{2\sqrt{\alpha}}\right)}\left(1-\exp\left(-2\left[\sqrt{\alpha}\cos\phi - \frac{d_N}{2}\right]^2\right)\right), \tag{3.41}$$

where ξ is the linear beam-beam tuneshift parameter and the prime denotes a derivative with respect to J.[29]

For head-on collisions, the amplitude of the resonance for various even-ordered resonances is shown in Figure 3.4 and 3.5. Both figures normalize the resonance amplitude to the beam-beam tune shift parameter. Figure 3.4 displays the absolute value of the resonance amplitude in the more familiar logarithmic scale seen in much of the literature (See Evans (1983) or Peggs (1986), for example). Figure 3.5 is the resonance amplitude plotted on a linear scale. It is evident in both of these figures that the absolute magnitude of the resonant component of the beam-beam perturbation is greater for lower order resonances than for higher order resonances. This is true for a particle at any oscillation amplitude.

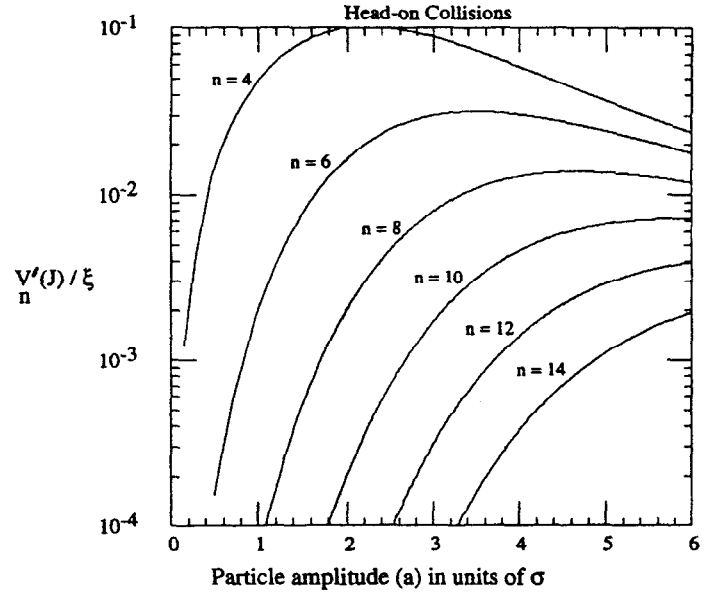

Figure 3.4: Absolute value of the amplitude of a beam-beam driven resonance of order n for head-on collisions. A round beam approximation is used.

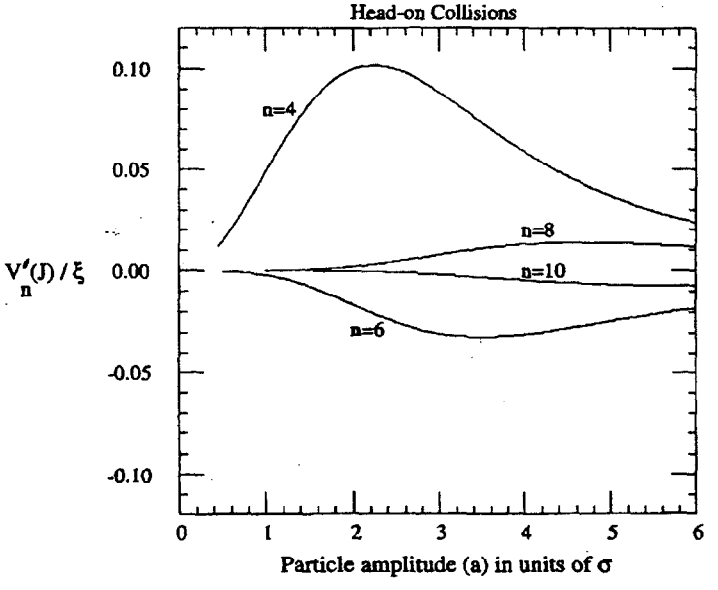

Figure 3.5: Amplitude of a beam-beam driven resonance of order n for head-on collisions. A round beam approximation is used.

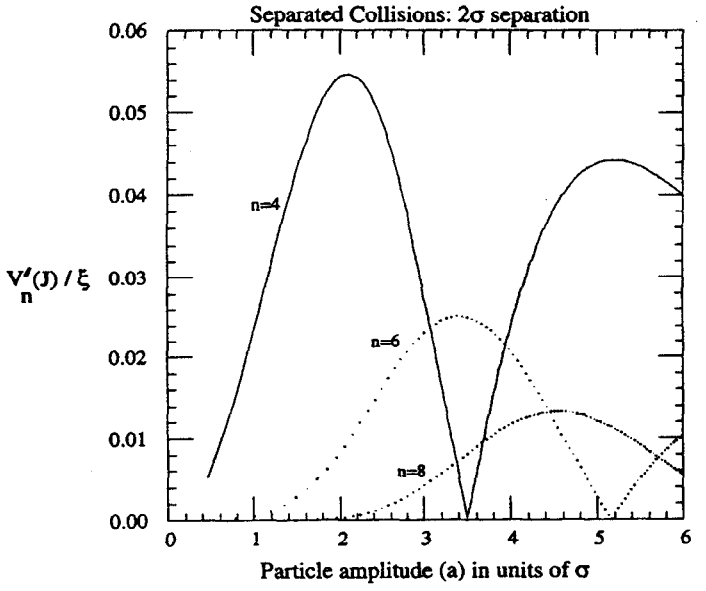

Figure 3.6: Absolute value of the amplitude of a beam-beam driven resonance of order n for a beam separation of 2σ. A round beam approximation is used.

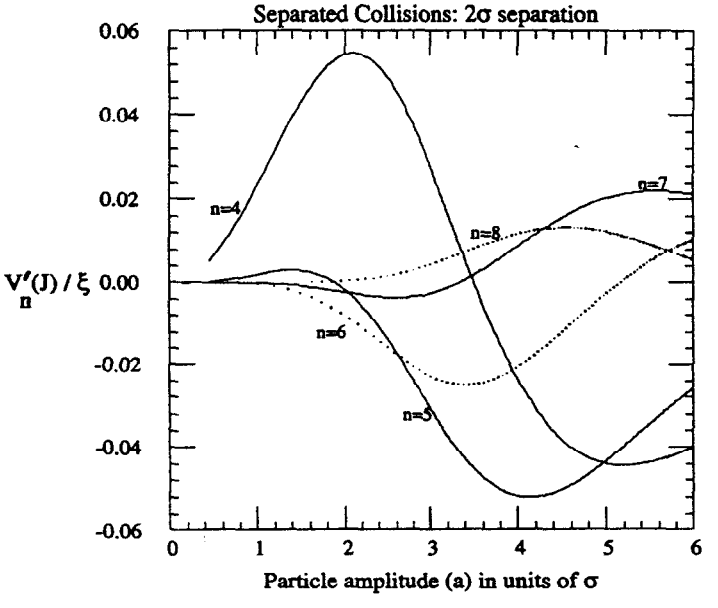

Figure 3.7: Amplitude of a beam-beam driven resonance or order n for a beam separation of 2σ. A round beam approximation is used.

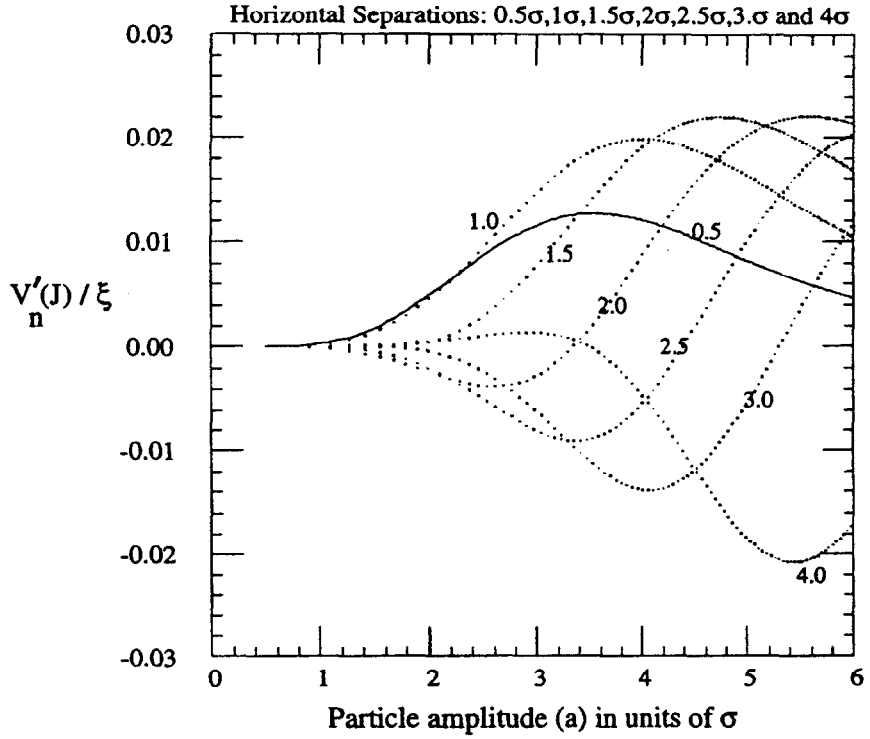

Figure 3.8: Amplitude of a beam-beam driven resonance of $7th$ order for different horizontal separations. A round beam approximation is used.

A non-zero separation introduces resonant components of the beam-beam force which drive odd-ordered resonances. For a separation of 2σ, the resonance amplitude is plotted for some odd and even-ordered resonances in Figure 3.6 and Figure 3.7. Although driving terms from lower order resonances have a maximum oscillation amplitude which is larger than higher order resonances, it is no longer possible to generalize that the amplitude of a beam-beam resonant driving term is larger for lower order resonances. A particle oscillating at a given amplitude may in fact see a larger resonance excitation near a higher order resonance.

The dependence of resonance amplitude on beam separation is shown in Figure 3.8 for a seventh order resonance.

3.5 BEAM-BEAM SIMULATIONS

In order to predict a particle's behavior in the presence of the beam-beam interaction in the Tevatron, a simulation code was developed to calculate the predicted position and phase of a particle after a designated number of turns. The simulation code is descendant from simulation code originally written by Werner Herr.[34][35]

The model used for the simulation is concerned only with particle motion due to the beam-beam interaction. The motion of a particle between beam-beam crossing points is assumed to be linear motion and coupling between the two transverse planes is not taken into account. The particle experiences an angular kick due the beam-beam interaction at each beam-beam crossing point. The simulation code is summarized below.

Given a particle's initial position and phase at a location 1 in a collider, a linear propagation to location 2 is described by

$$\begin{pmatrix} x_2 \\ x_2' \\ y_2 \\ y_2' \end{pmatrix} = M_{12} \begin{pmatrix} x_1 \\ x_1' \\ y_1 \\ y_1' \end{pmatrix}. \tag{3.42}$$

The transfer matrix M is defined by the lattice parameters in the horizontal and vertical planes at the corresponding locations [9]:

$$M_{12} = \begin{pmatrix} m_x & 0 \\ 0 & m_y \end{pmatrix}, \tag{3.43}$$

where m_x and m_y are given by Equation 2.13. The simulation assumes the motion of a particle from one beam-beam collision point to the next is a linear motion as described above. The phase advance from a beam-beam crossing point (1) to the next crossing point (2) is given by

$$\Delta\phi = \phi_2 - \phi_1 = 2\pi\Delta Q_{21}. \tag{3.44}$$

At each beam-beam interaction point, a beam-beam kick of magnitude $\Delta x'$ and $\Delta y'$ is added to a particle's phase. The beam-beam kick expression of Equation 3.5 is generalized to non-round beams in the simulation. For computational purposes, the vertical kick in the simulation is given by

$$\begin{aligned} \Delta y' \;=\; & -\frac{2N_b r_p y}{\gamma}\sqrt{\frac{2\pi}{a^2-b^2}}\cdot \\ & \mathcal{R}\left[w\left(\frac{x+iy}{\sqrt{2(a^2-b^2)}}\right) - \exp\left[\left(-\frac{x^2}{2a^2}-\frac{y^2}{2b^2}\right)\right] w\left(\frac{x\frac{b}{a}+iy\frac{a}{b}}{\sqrt{2(a^2-b^2)}}\right)\right] \end{aligned} \tag{3.45}$$

for $a > b$.[38] The parameters a and b denote the horizontal and vertical bunch sizes of the colliding proton distribution. The function $w(A+iB)$ is the complex error function.

The horizontal kick is given by the imaginary part of the square brackets. The use of an algorithm to calculate the complex error function using an asymptotic approximation and Pade approximations decreased computation time significantly.[39]

When a non-zero beam separation is present at a collision point, care must be taken in calculating the beam-beam kick.[36] Consider a beam-beam collision with a non-zero separation d in the horizontal plane. The beam-beam potential of Equation 3.13 is

$$V(x,y) = C \int dt \frac{1 - e^{-\left(\frac{(x-d)^2}{2\sigma_x^2+t} + \frac{y^2}{2\sigma_y^2+t}\right)}}{\sqrt{(2\sigma_x^2+t)(2\sigma_y^2+t)}} \tag{3.46}$$

where $C = Nr_p/\gamma$. The kick from this potential is

$$\begin{aligned} \Delta x' &= \frac{\partial V}{\partial x} \\ &= C(x-d) \int dt \frac{e^{-\left(\frac{(x-d)^2}{2\sigma_x^2+t} + \frac{y^2}{2\sigma_y^2+t}\right)}}{\sqrt{(2\sigma_x^2+t)^{3/2}(2\sigma_y^2+t)^{1/2}}}. \end{aligned} \tag{3.47}$$

For zero amplitude particles, this expression becomes

$$\Delta x' = Cd \int dt \frac{e^{-\left(\frac{d^2}{2\sigma_x^2+t}\right)}}{\sqrt{(2\sigma_x^2+t)^{3/2}(2\sigma_y^2+t)^{1/2}}} \tag{3.48}$$

which is merely a dipole kick. This dipole kick will result in a shift in the closed orbit of the particle. In order to calculate a particle's tune, it is necessary to calculate the gradient of the kick around the closed orbit of the particle, i.e. x=0. The approximation of Equation 3.8, $q = \Delta x'/x$, which was used in the head-on collision case is no longer valid. The valid expression is

$$q = \frac{\partial(\Delta x')}{\partial x}. \tag{3.49}$$

The change in a particle's closed orbit due to the constant dipole kick is negligible for small kicks, but the change is large for sizeable kicks. A large dipole kick will change a particle's reference system. A subtraction of the dipole kick is necessary to bring the reference system back. The beam-beam kick used in the simulation code is obtained by subtracting out the dipole kick contribution;

$$\Delta x'_{total} = \Delta x'(y+d) - \Delta x'(d). \tag{3.50}$$

This beam-beam kick expression will give a correct calculation of the beam-beam tune shift of a particle. If the dipole contribution is not subtracted, small amplitude particles will assume much larger amplitudes. These particles will then start betatron oscillations with larger

amplitudes than their original amplitudes and start to sample a different amplitude of the opposing beam. In reality, the particles oscillate with the same betatron amplitudes but at different closed orbits. The tune change is thus

$$\Delta Q \propto q = C\frac{\partial}{\partial x}\left((x-d)\int dt \frac{e^{-\left(\frac{(x-d)^2}{2\sigma_x^2+t}+\frac{y^2}{2\sigma_y^2+t}\right)}}{\sqrt{(2\sigma_x^2+t)^{3/2}(2\sigma_y^2+t)^{1/2}}}\right) \tag{3.51}$$

and

$$\Delta Q \propto q = C\int dt \frac{e^{-\left(\frac{(x-d)^2}{2\sigma_x^2+t}+\frac{y^2}{2\sigma_y^2+t}\right)}}{\sqrt{(2\sigma_x^2+t)^{3/2}(2\sigma_y^2+t)^{1/2}}} - 2C(x-d)^2\int dt \frac{e^{-\left(\frac{(x-d)^2}{2\sigma_x^2+t}+\frac{y^2}{2\sigma_y^2+t}\right)}}{\sqrt{(2\sigma_x^2+t)^{5/2}(2\sigma_y^2+t)^{1/2}}} \tag{3.52}$$

For $x = 0$, the linear tune shift is

$$\Delta Q \propto q = C\int dt \frac{e^{-\left(\frac{d^2}{2\sigma_x^2+t}+\frac{y^2}{2\sigma_y^2+t}\right)}}{\sqrt{(2\sigma_x^2+t)^{3/2}(2\sigma_y^2+t)^{1/2}}} - 2Cd^2\int dt \frac{e^{-\left(\frac{d^2}{2\sigma_x^2+t}+\frac{y^2}{2\sigma_y^2+t}\right)}}{\sqrt{(2\sigma_x^2+t)^{5/2}(2\sigma_y^2+t)^{1/2}}} \tag{3.53}$$

The first term is the well known classical part. The second term can cause the tune shift to become negative after a certain separation d.

Figure 3.9 illustrates the beam-beam tune shift vs. separation as computed by the simulation code. The horizontal and vertical tune shift due to one beam-beam collision is shown for a small amplitude $(0.001\sigma_x, 0.001\sigma_y)$ and a large amplitude $(2\sigma_x, 2\sigma_y)$ particle. The operating tune for the above simulation runs was in a "resonance free" region of tune space; a region absent of lower order resonances.

It is of interest in this work to compare beam-beam simulations to particle losses. In this case, the absolute position of a particle at a given location in the ring is important. The orbit offset due to the dipole kick which is subtracted from the beam-beam kick during particle tracking must be taken into account. The dipole kick causes a particle to orbit on a new closed orbit. All amplitude particles in a particle distribution are kicked equally by the dipole kick. It is sufficient to calculate the additional orbit offset which results from the dipole kick and add this orbit offset to that measured during tracking.[44] The closed orbit offset is calculated using Equation 2.35.

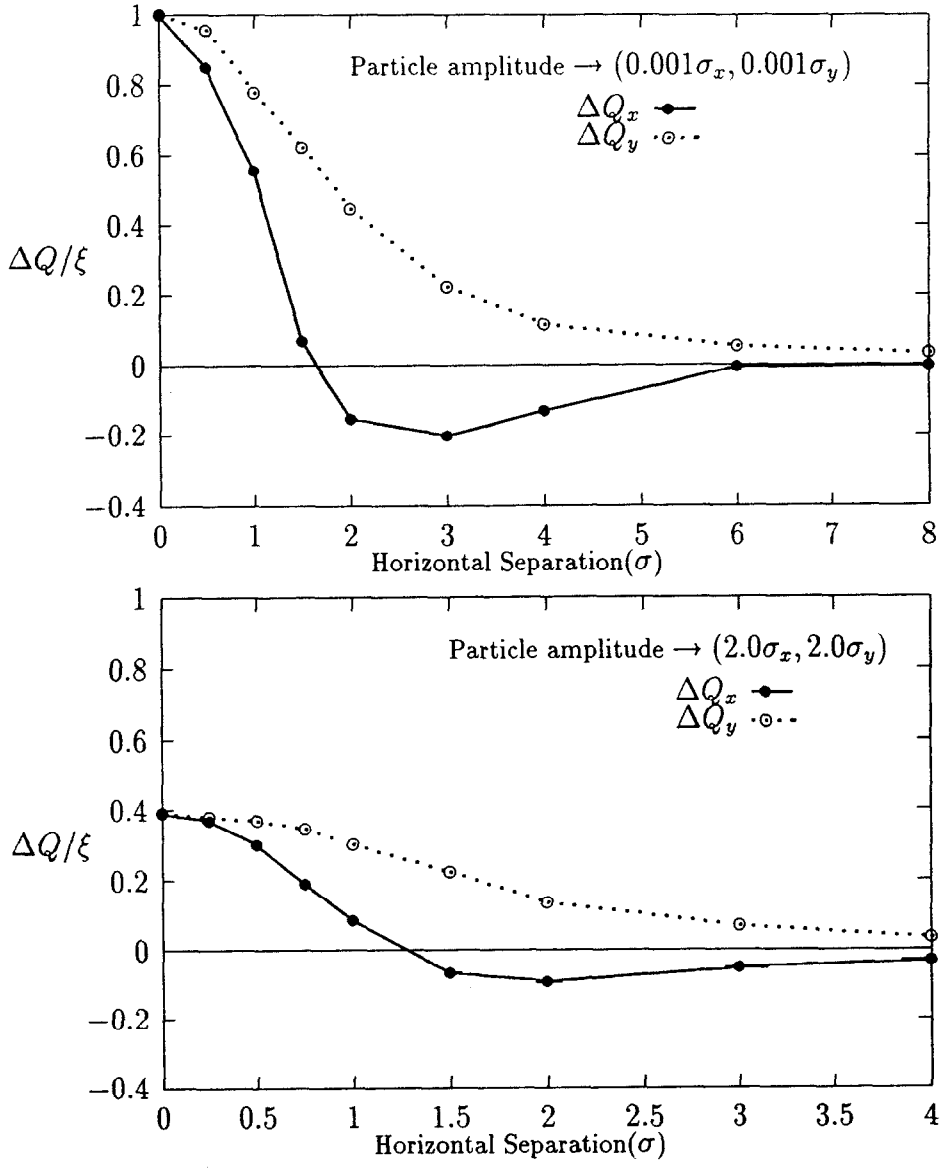

Figure 3.9: Simulation results of the tune shift of a small and large amplitude particle in the presence of a non-zero horizontal separation.